Improving Machine Learning Predictions of Metallic Glass Forming Ability

By

Benjamin T. Afflerbach

A dissertation submitted in partial fulfillment of

the requirements for the degree of

Doctor of Philosophy

(Materials Science and Engineering)

at the

UNIVERSITY OF WISCONSIN-MADISON

2021

Date of final oral examination: 08/16/2021

The dissertation is approved by the following members of the Final Oral Committee:

Dane Morgan, Professor, Materials Science and Engineering
Izabela Szlufarska, Professor, Materials Science and Engineering
Paul Voyles, Professor, Materials Science and Engineering
John Perepezko, Professor, Materials Science and Engineering
Victor Zavala, Professor, Chemical and Biological Engineering

Thesis Abstract

Since the discovery of metallic glass alloys in 1959, there has been a continuous drive from the scientific community to understand and predict the glass forming ability of new alloys. This drive has led to the evolution of alloys from the first metallic glasses, which required ultra-rapid quenching and could only be synthesized in thin ribbons or fine powder, to bulk metallic glasses which can be synthesized into relatively large ingots via more traditional metallurgical techniques. These glasses have demonstrated useful properties in a variety of applications driving interest for the discovery of new metallic glass alloys. To predict the glass forming ability of potential new alloys simple rules of thumb that initially served as basic screening devices have evolved into more complex modelling approaches. In the past decade advances in computing and the quantity of available data, machine learning has increasingly been an appealing tool for making predictions of metallic glass forming ability due to its ability to learn complex relationships and make new predictions rapidly. This thesis develops two methods for improving machine learning predictions of glass forming ability.

The first in through development of molecular dynamics features for use in machine learning models. Previous machine learning efforts have utilized features which are either very high quality but very inaccessible, or lower quality but very accessible. This tradeoff has meant some models are extremely hard to make new predictions with (inaccessible features), and others must sacrifice predictive ability (low quality features). Using hi-throughput molecular dynamics simulations we obtain 9 features which improve model's predictive ability at a fraction of the cost of previously developed feature sets.

The second focus of the work is developing methods for synthesizing experimental databases for training models. Starting with an initial database of less than one hundred experimental measurements of the critical cooling rate we use multiple techniques to construct a final glass forming ability database of more than 3,000 values which is then used to perform a wide search for new bulk metallic glasses. From this search seven alloys are identified as being of particular interest as novel bulk metallic glasses.

Acknowledgments

Throughout my time here in Madison, I've met and been influenced by a number of people who without their support, feedback, and example I would not be where I am today.

First, I would like to thank my advisor Professor Dane Morgan for his guidance and patience throughout my graduate career. Coming directly from a bachelor's in mechanical engineering, with little computational materials science knowledge, I struggled to find my feet initially. Without Dane's continued support I would not be where I am today. I am especially grateful for the many opportunities as well to pursue teaching and scientific outreach activities along with my research. I'd also like to thank Prof. Izabela Szlufarska, Prof. Paul Voyles, Prof. John Perepezko, and Prof. Victor Zavala for being on my thesis committee and providing valuable feedback.

This work would not have been possible without support from NSF DMREF award number DMR-1332851, National Science Foundation Software Infrastructure for Sustained Innovation (SI2) award number 1148011, and NSF DMREF award number DMR-1332851. This work used the Extreme Science and Engineering Discovery Environment (XSEDE), which is supported by National Science Foundation grant number ACI-1548562. This work used the Extreme Science and Engineering Discovery Environment (XSEDE) Stampede through allocation TG-DMR090023. This research was also performed using the compute resources and assistance of the UW-Madison Center for High Throughput Computing (CHTC) in the Department of Computer Sciences. The CHTC is supported by UW-Madison, the Advanced Computing Initiative, the Wisconsin Alumni Research Foundation, the Wisconsin Institutes for Discovery, and the National

Science Foundation, and is an active member of the Open Science Grid, which is supported by the National Science Foundation and the U.S. Department of Energy's Office of Science.

I would like to thank Dr. Henry Wu, Dr. Tam Mayeshiba, and Dr. Ryan Jacobs who provided me with advice and guidance during my first years in the Computational Materials Group as senior members of the group. The example set by them was a consistent reminder of things to strive for.

Throughout my time here there have been several people who have had a great impact on my professional development. Thank you to Dr. Matthew Stilwell and Dr. Anne Lynn Gillian-Daniel for their input, feedback, and eye-opening discussions about scientific education.

I couldn’t have made it without the friends I have made here in Madison, and specifically the DnD group. I look forward to every time we get to sit down and tell stories together.

Finally, I would like to thank my family. My parents Mary and Tom, who have suffered through many (hopefully improving!) explanations and rambling about my research. And my sisters, who have been a constant inspiration as they have pursued their own careers. I love you all and cannot wait until we are able to get all of us in one place again!

List of Papers

1. **B.T. Afflerbach**, C. Francis, L. Schultz, J. Erickson, V. Meschke, E. Strand, L. Ward, J. Perepezko, D. Thoma, P.M. Voyles, I. Szlufarska, D. Morgan, Machine Learning Prediction of Critical Cooling Rate for Metallic Glasses from Expanded Datasets and Elemental Features (**Submitted, Nature Communications)**
2. **B.T. Afflerbach**, L. Schultz, J.H. Perepezko, P.M. Voyles, I. Szlufarska, D. Morgan, Molecular simulation-derived features for machine learning predictions of metal glass forming ability, Comput. Mater. Sci. 199 (2021) 110728. doi:10.1016/j.commatsci.2021.110728.
3. L.E. Schultz, **B. Afflerbach**, C. Francis, P.M. Voyles, I. Szlufarska, D. Morgan, Exploration of characteristic temperature contributions to metallic glass forming ability, Comput. Mat. Sci. 196 (2021). 110494. doi:10.1016/j.commatsci.2021.110494.
4. R. Jacobs, T. Mayeshiba, **B. Afflerbach**, L. Miles, M. Williams, M. Turner, R. Finkel, D. Morgan, The Materials Simulation Toolkit for Machine learning (MAST-ML): An automated open source toolkit to accelerate data-driven materials research, Comput. Mater. Sci. 176 (2020). doi:10.1016/j.commatsci.2020.109544.
5. Y.-C. Liu, **B. Afflerbach**, R. Jacobs, S.-K. Lin, D. Morgan, Exploring effective charge in electromigration using machine learning, MRS Commun. 9 (2019). doi:10.1557/mrc.2019.63.
6. H.-J. Lu, N. Zou, R. Jacobs, **B. Afflerbach**, X.-G. Lu, D. Morgan, Error assessment and optimal cross-validation approaches in machine learning applied to impurity diffusion, Comput. Mater. Sci. 169 (2019). doi:10.1016/j.commatsci.2019.06.010.

List of Presentations

1. **Afflerbach B.**, "An Introduction to Machine Learning for Materials Science: A Basic Workflow for Predicting Materials Properties", 2021 Summer Bootcamp, Online, July 14, 2021
2. **Afflerbach B.**, "An Introduction to Machine Learning for Materials Science: A Basic Workflow for Predicting Materials Properties", Hands-on Data Science and Machine Learning Training Series, Online, May 12, 2021
3. **Afflerbach B**., Schultz L., Francis C., Erickson J., Thoma D., Voyles P., Szlufarska I., Morgan D. (2020, Nov. 27). *Machine Learning Predictions of Glass Forming Ability from Compositional Information* [Conference Presentation] Materials Research Society Conference, Virtual.
4. **Afflerbach B**., Jacobs R., Morgan D., (2020, May 26). *Overview of Data Science Programs, Materials, and Tools*. [Workshop Presentation] Midwest BD Spoke/CHiMaD Workshop, Virtual.
5. **Afflerbach B**., Schultz L., Szlufarska I., Morgan D., (2019, Sept. 29 – Oct. 3). *Exploring Molecular Dynamics Features to Improve Machine Learning Predictions of Glass Forming Ability*. [Conference Presentation] Materials Science and Technology Conference, Portland, Oregon, United States.
6. **Afflerbach B**., Mayeshiba T., Jacobs R., Li W., Wu H., Schultz L., Liu Y., Shen M., Morgan D., (2019, June 5). *Standardized Machine Learning Software to Enable Rapid Iteration of Materials Science Research*. [Poster Presentation] MADLab / AFRL Machine Learning Technical Exchange, Madison, WI, United States.
7. **Afflerbach B**. Jacobs R., Morgan D., (2018, Aug. 2). *The Materials Simulation Toolkit for Machine Learning (MAST-ML)*. [Conference Presentation and

Workshop Activity] Machine Learning for Materials Research (MLMR) & Workshop on Machine Learning Quantum Materials, College Park, MD, United States.

8. **Afflerbach B**., Mayeshiba T., Jacobs R., Li W., Wu H., Morgan D., (2017, Oct 15-16). *Standardized Machine Learning Software to Enable Rapid Iteration of Materials Science Research*. [Conference Talk and Poster Presentation] Regional Materials and Manufacturing Network (RM2N) Conference, Platteville, WI, United States.

Table of Contents

List of Figures

List of Tables

List of Abbreviations

BCC: Body centered cubic

BMG: Bulk metallic glass

CNA: Common neighbor analysis

CNT: Classical nucleation theory

CTs: Characteristic temperatures

CV: Cross validation

DFT: Density functional theory

EAM: Embedded atom method

FCC: Face centered cubic

HCP: Hexagonal close packed

ICO: Icosahedral cluster

MAST-ML: Materials simulation toolkit for machine learning

MD: Molecular dynamics

MG: Metallic glass

ML: machine learning

Pymatgen: Python materials genome library

RMSE: Root mean squared error

VASP: Vienna ab-initio simulation package

VP: Voronoi polyhedra

Chapter 1. General Introduction and Motivation

1.1. Chapter Summary

This thesis is comprised of a total of seven chapters. This chapter serves as an introduction to the work, providing motivation for the studies discussed in later chapters. Chapter 2 provides a more in-depth background on key methods used in this work. Chapter 3 covers our work on developing computationally accessible features for use in machine learning models of glass forming ability (GFA). Chapter 4 details methods for synthesizing improved GFA databases for model training. We also propose and demonstrate methodologies for predicting new bulk metallic glasses (BMG) from the machine learning (ML) models trained. Chapter 5 gives a brief overview of other collaborative research efforts that do not fall under the main focus of metallic glasses but highlight additional machine learning results and lessons learned. Chapter 6 outlines a number of research mentoring projects with a focus on mentoring undergraduate researchers. These studies again have a focus on machine learning however do not fall under the main focus of metallic glasses. Finally, Chapter 7 contains a summary of the main studies in Chapter 3 and Chapter 4, and makes suggestions for possible future work.

1.2. What are metallic glasses?

Metallic Glasses (MGs) are amorphous solids identified by their lack of any long-range order. They are traditionally synthesized by quenching a liquid metal rapidly to avoid nucleation of crystalline phases, undergoing the glass transition, and resulting in an amorphous solid. There are several other processes for forming a metallic glass such as mechanical alloying [1] and sputtering [2,3] however in the context of this work we will

focus on glasses that are synthesized directly from rapid quenching of a liquid melt. The change in structure from previous crystalline metals opened up an entirely new class of metal alloys with their discovery over 60 years ago.

MGs have been discovered with a number of unique properties that have driven interest in developing the class of metals further. There are MGs with high strength and high elastic limit, high resistance to wear and corrosion, soft-magnetic properties, and excellent biocompatibility [4–13]. These properties have supported a wide range of application spaces including biomaterials, magnetic devices, surface coatings, MEMS devices, and structural materials [14–16]. However, even with the development of MGs with functional properties they are still not widely used. This is primarily due to the overall relatively poor glass forming ability (GFA) of metals compared to more common glassy materials such as oxide glasses. This is further compounded by an extreme scarcity of high GFA alloys. Therefore, a key challenge in MG materials discovery is identification of MG forming compositions in existing glassy alloys and discovery of entirely new MG alloys.

The GFA of an alloy is a general term for the ease of forming MGs. There are a number of different metrics that can be used to quantify this property and they each have tradeoffs in the fidelity of information they contain and their ease of acquisition. The most direct measure of GFA is the critical cooling rate (R_C) shown schematically in *Figure 1.1*. On a Continuous Cooling Transformation (CCT) diagram the slowest cooling rate which avoids passing into the crystal region is called defined as R_C. Once below the glass transition temperature (T_g) the undercooling melt vitrifies, and the final glassy state is obtained. Along with being the most direct metric, the R_C is also hardest GFA metric to

measure directly, especially for materials with poor GFA. R_C values can range over many orders of magnitude, from bulk metallic glasses (BMG) which have R_C values below 10^3 K/s, to melt-spun glasses that can go up to 10^6 K/s, to what would be considered non-glass forming alloys with R_C values estimated around 10^{10} K/s. Experimental techniques to directly measure these values are limited to state-of-the-art calorimetry such as flash-DSC which can access the necessary cooling rates to suppress crystallization.

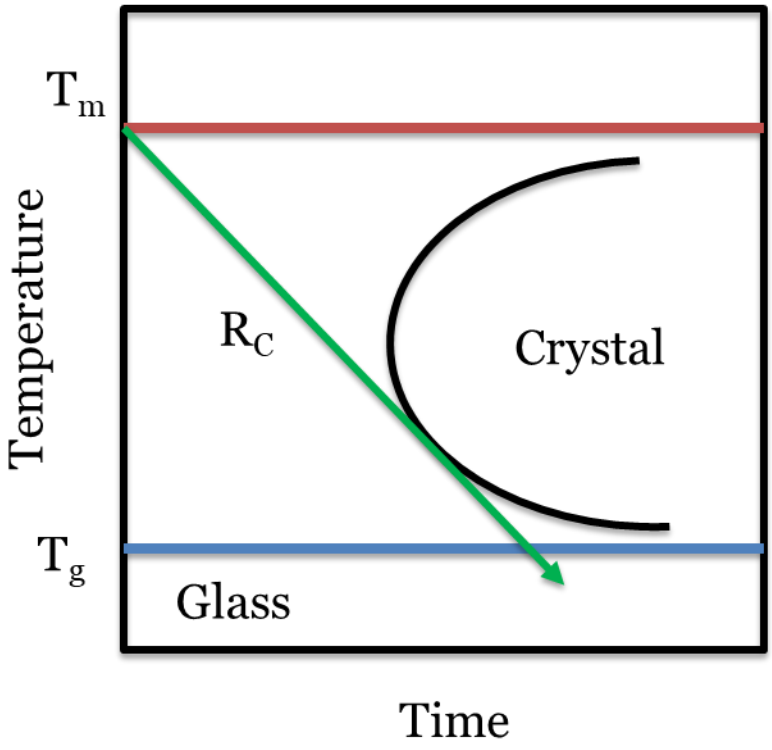

Figure 1.1. Schematic Continuous Cooling Transformation (CCT) curve for identifying the critical cooling rate to avoid crystallization.

The critical casting diameter (D_C) is another common metric for quantifying GFA. It is also referred to as critical casting thickness, depending on the geometry of the mold. Similar in spirit to R_C it is the largest size of a MG that is able to be cast before nucleating crystals. Traditionally this is done in a copper mold, though there are other methods and

materials used as well. This also leads to the term bulk metallic glass (BMG). BMGs are fairly arbitrarily defined to be MGs with a D_C values above 1 mm. Occasionally some researchers may make different cutoffs for what they consider "bulk", but 1 mm is the most widely used cutoff. The D_C is a less direct measure of the intrinsic GFA of an alloy because it includes heterogenous nucleation effects as well as homogenous nucleation. However, it is significantly easier to obtain than R_C and therefore there are significantly more measurements of it in the literature [17].

The last widely popular method for measuring GFA is tied to a third type of experiment, melt-spinning. In melt-spinning a continuous stream of molten metal is deposited on a large, spinning, chilled copper wheel. As the thin stream of metal cools a continuous ribbon of materials is formed, and these glasses may also be called ribbon glasses. There is some degree of change is effective cooling rate that can be achieved by manipulated the flow rate of the metal and the wheel speed, but melt-spun glasses are typically cooling at a rate of between 10^4 K/s and 10^6 K/s. Melt-spinning has been used to perform wide searches for potential MGs due to the speed of sample synthesis. However, it is the downside that it only gives a binary metric of GFA, in that either it did or did not form a MG under the melt-spinning conditions.

1.3. Previous methods to understand glass forming ability

Methods for discovery of BMGs have generally fallen into two broad categories. The first category is qualitative predictions of good glass forming ability (GFA) alloys and regions through identification of various qualitative and semi-quantitative physics-based criteria (e.g., deep eutectics) such as those outlined by Inoue et al [4]. This methodology

has had many successes and is responsible for the discovery of many of the BMG alloys known today. The second category is models that quantitatively predict a metric of GFA such as the critical cooling rate (R_C) or the critical casting diameter (D_c). As our understanding of glassy alloys, and the amount of available data increases, these quantitative models are becoming more appealing as they can potentially reveal much more detailed information about the GFA across alloys.

Quantitative GFA predictions take many forms but can be organized by their choices of features, models, and target predictions. Features typically range from approximately instantly accessible (e.g., elemental properties [18]) to moderately accessible properties needing some calculation (e.g., thermodynamic properties determined from CALPHAD [19], or liquid properties determined by molecular dynamics [20]) to properties requiring extensive synthesis and characterization (e.g., glass transition temperature [17] or fragility [21]). Models range from simple linear functions (e.g., the R_C vs. omega correlations [17]) to fully non-linear machine learning models (e.g., D_c vs features fit with boosted trees [22]). Target values range from qualitative categorical predictions (e.g., is a glass under melt spinning [23]) to quantitative models of R_C [17] and D_c [22,24].

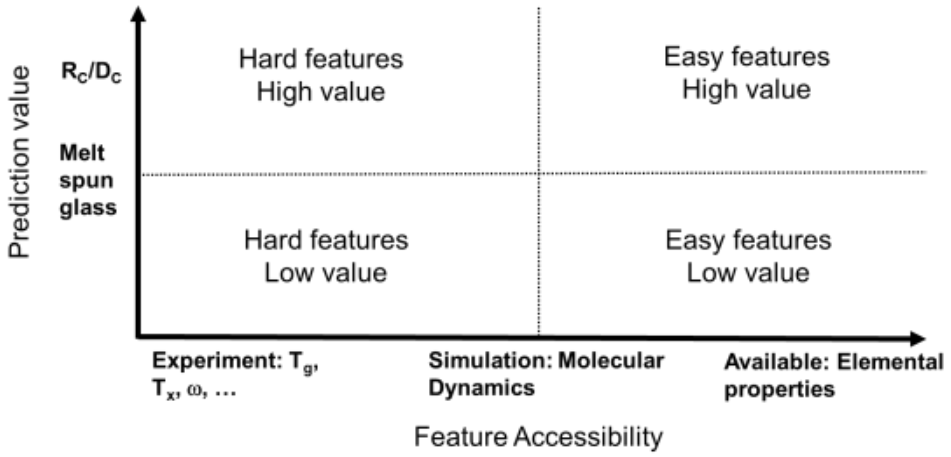

Figure 1.2. Summary of predictive models by feature accessibility and predictive value.

A summary of these distinctions is given in *Figure 1.2* in which modeling effort are divided on two axes, Feature accessibility and Predictive Value. As discussed in the previous paragraph there has been success in probing the upper left quadrant of the plot through developing features which require extensive time and effort to access. And there has also been success in developing models which use only readily accessible features to predict the lower right quadrant. However, there has not been success in pushing both of these quadrants towards the upper right by maintaining high accessibility in features, and direct predictions of glass forming ability. In this thesis we pursue two techniques to move our models in this direction by developing more accessible features that can be obtained from high throughput simulations, and extension of existing experimental databases which has increased available training data for models by an order of magnitude.

Chapter 2. Computational Methods

In this chapter we will introduce the core computational techniques used in this thesis. The primary simulation technique used is classical molecular dynamics by which we can directly simulation the behavior of metallic glasses under a variety of conditions. The method is used in Chapter 3 to both generate a computation database of critical cooling rates as well as then extract properties of the resulting metallic glasses. The main machine modeling results focus on two model types, random forest and LASSO regression models. We will introduce their working principles and benefits.

2.1. Molecular Dynamics

Molecular dynamics (MD) is a computer simulation method for studying materials on the atomic scale by dynamically evolving a many-body system. The method was developed by Fermi et al. [25], Alder et al.[26], and Rahman et al. [27] who evolved the method from studies of hard spheres to the first study on a real material, liquid argon. MDs basic operating principle is to solve Newton's equations of motion to model the motion of classical particles such as atoms and molecules.

$$m_i \frac{d^2\vec{r_i}}{dt^2} = \sum_{i \neq j} \overrightarrow{F_{ij}} + \overrightarrow{F_i^e} \qquad (2.1)$$

Where m_i and r_i are the mass and position of atom i, F_{ij} is the interatomic force between atom i and atom j, and F_i^e is any external force on atom i. By integrating numerically over a small time step Δt atomic positions can be evolved over time to simulate the motion of atoms. Δt is typically around 1 fs to ensure that each step is well below typic vibrational

frequencies of the atoms being simulated. One common method for integration is the Velocity-Verlet algorithm which takes the form of

$$\vec{r_i}(t+\Delta t) = \vec{r_i}(t) + \vec{v_i}(t)\Delta t + \frac{\vec{F_i}(t)}{2m_i}(\Delta t)^2 \qquad (2.2)$$

$$\vec{v_i}(t+\Delta t) = \vec{v_i}(t) + \frac{\vec{F_i}(t)+\vec{F_i}(t+\Delta t)}{2m_i}(\Delta t) \qquad (2.3)$$

where $\vec{v_i}$ is the velocity of atom i and $\vec{F_i}$ is the total force acting on atom i.

With the previous three equations established the only major thing missing before an MD simulation could be performed is defining the interaction between the atoms. In classical MD this interaction is usually calculated from the gradient of the interatomic potential energy

$$\overrightarrow{F_{ij}} = -\nabla U_{ij}\left(\overrightarrow{r_{ij}}\right) \qquad (2.4)$$

where $U_{ij}\left(\overrightarrow{r_{ij}}\right)$ is the interatomic potential energy between atom i and j. With this formalism the forces can be calculated directly from the positions of all of the atoms, closing the loop on an iterative stepping procedure that with a known set of positions and velocities can calculate the forces on each atom and then update the positions and velocities for the next time step.

For this work simulation have be run using Embedded Atom Potentials (EAM) [28] are used to simulate metallic glass behavior under a variety of conditions. In the EAM potential the potential energy of an atom i is given by

$$E_i = \Phi_{t_i}\left(\sum_{i\neq j}\rho_{t_j}(r_{ij})\right) + \frac{1}{2}\sum_{i\neq j}\phi_{t_i t_j}(r_{ij}) \qquad (2.5)$$

where t_i represents species of atom i, r_{ij} is the distance between atoms i and j, ρ_{t_j} is the contribution to the electron charge density from atom j at the position of atom i, Φ_{t_i} is the embedding function energy that is required to place atom i into the electron cloud, and $\phi_{t_i t_j}$ is a pairwise potential function. The fitting of these potentials is beyond the scope of this thesis. See Chapter 3 for more details on the simulations performed.

2.2. Machine learning modeling

2.2.1. Random forest models

Random Forests (RF) are a popular ensemble machine learning model originally proposed by Tin Kam Ho in 1995 [29] with the goal of improving upon the single decision tree model. Decision trees, shown schematically in *Figure 2.1*, are attractive models due to their high execution speed. However, they cannot be grown to arbitrary complexity without suffering from a loss of generalizability and overfitting to training data. Therefore, one of the primary goals of introducing the RF type model was to combat this overfitting by training many individual decision trees which can compensate for each individual tree's errors, allowing the growth of more complex trees which can capture more complex relationships between input features and target predictions.

The basic structure of a single tree can be described starting from the Root node at the top of the tree. The model proceeds in one direction from top to bottom, making a single split at each node that isn't a leaf node. At the root node and each decision node a feature is assigned to the node as well as a value to split on. This pair of feature and value

(e.g., melting temperature < 1,000 K) can be referred to as a decision rule. A trained model consists of a defined structure of Root, Decision, and Leaf nodes; with a decision rule assigned to each Root and Decision node, and a prediction assigned to each Leaf node. From this structure we can see how a prediction can be made from a single decision tree by following the decision path outlined by a specific set of input features that are tested at each node.

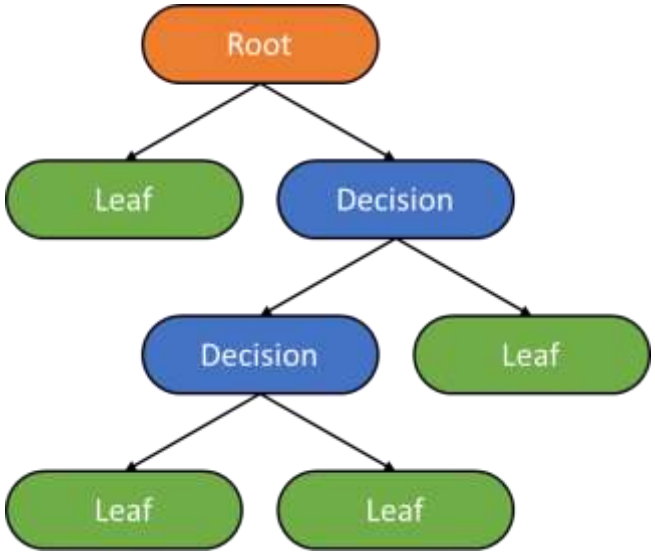

Figure 2.1. Schematic decision tree structure identifying Root, Decision, and Leaf nodes.

With this structure we can then see how a RF model and all of its subcomponent decision trees are trained. The simplest set of training steps for each tree is to first start at the root node and consider every possible combination of features and values as the decision rule for that node and pick the one that minimizes a chosen error metric (e.g., mean squared error for regression) for all of the training data. With that decision rule locked in, proceed to the next layer of the tree and repeat the search again for the reduced set of training data that applies to each node. Then stop once a stopping criterion is met

(e.g., maximum tree depth, minimum number of training points at the node). With this procedure error is minimized at each layer in the tree in a greedy search to try to minimize the overall error. It is important to notice however that with the procedure above each of the trees trained in the RF model would be identical. This is where two additions to the RF model formalism come into play. These are the concepts of bagging and random selection of Features introduced by Breiman and Cutler [30,31]. Bagging is the process of training each individual decision tree on a different subset of the total training set with replacement. Random selection of features is the same, but a random subset of features is chosen each time to train on. These additions seek to minimize the correlation between each tree in the forest allowing the model to better compensate for overfitting in individual trees.

With these methods for setting up the structure and training of random forest models it is useful to highlight some best practices and guidance for using RF models. One of the biggest benefits to working with RF models is their ease of optimization. In all of the results shown in this thesis a strategy of training complex trees with few or no limits on their growth has led to the best performance. In all cases a rough grid search was applied over relevant hyperparameters and they all led to reduced performance when growth was limited. In practice this means hyperparameters such as the maximum depth of trees that would control growth and need to be finely optimized in a single decision tree, can be set to their upper / lower bound in the case of RF models (e.g., Max depth = None). This ability to quickly get a well behaved model means RFs can be extremely appealing when trying to quickly assess differences in other aspects of machine learning such as differences in feature sets, data sets, or prediction types.

2.2.2. LASSO models

The Least Absolute Shrinkage and Selection Operator (LASSO) is an extension to linear regression models proposed in 1995 by Robert Tibshirani [32]. As originally proposed The LASSO minimizes the residual sum of squares subject to the sum of the absolute value of the coefficient being less than a constant. The LASSO model minimizes

$$\min_{B} \|y - BX\|_2^2 + \lambda\|B\|_1 \qquad (2.6)$$

where λ is regularization parameter, B is the vector of coefficients, y is the vector of target values, and X is the matrix of features and values for each data point. The left side of Eqn. $E(i) = \Phi_{t_i}\left(\sum_{i\neq j}\rho_{t_j}(r_{ij})\right) + \frac{1}{2}\sum_{i\neq j}\phi_{t_i t_j}(r_{ij})$ (2.5 is the basic form of linear regression. The addition of the regularization term on the right allows coefficients to shrink to and become explicitly 0, enabling the LASSO model to essentially perform an internal feature selection where it can ignore some features from the training data. This can improve interpretability of models as it is more readily apparent which features are the cause of model performance. This property is leveraged in Chapter 3 to identify promising computational features for predictions of glass forming ability.

LASSO is not the only extension of linear regression models that can perform some type of feature selection. Two other common techniques that are used are ridge regression and subset selection. Subset selection is the basic idea of fitting multiple linear regression models on various subsets of the overall feature set and identifying the best subset to fit a linear regression model to. At its simplest subsets can be tried in a greedy search starting from 1 feature and adding more, or starting with a full feature set and removing one at a time. These methods are referred to as “greedy” searches, and my iteratively comparing

performance after each addition / subtraction of features, an optimal set is hopefully obtained. The other primary method is using a ridge regression model. This model is structurally almost identical to the LASSO model apart from one difference. Instead of adding a regularization term in the form of an L1 norm, instead the L2 norm is used on the right-hand side of Eqn. $min_B \|y - BX\|_2^2 + \lambda\|B\|_1$ (2.6. This single change has the effect of allowing the LASSO model to explicitly set feature coefficients to 0, while the ridge regression model can set very low but non-zero coefficients.

Based on these properties of the LASSO model they are also fairly well behaved and there is not a significant time investment needed to obtain a well-fit model. Compared to the previous section on random forests the LASSO generally takes a similar amount of time to work with. The LASSO model is generally faster than a comparative RF model due to the simplicity of the model structure. This is especially true if the RF model has a large number of individual trees (e.g., > 200). However, the addition of the regularization hyperparameter means there is a necessary optimization step needed to identify the best performing value of λ. However, because there is just a single hyperparameter it is fairly trivial to perform a detailed grid search of values, assessing performance at each value to identify the optimal regularization. This ease of training, along with internal feature selection, and feature importance estimation, all within a very simple model structure are the main reasons it was used in the work in Chapter 3.

Chapter 3. Development of Computationally Accessible Molecular Dynamics Features

Note: This chapter has been published as B. Afflerbach, L. Schultz, J.H. Perepezko, P.M. Voyles, I. Szlufarska, and D. Morgan, "Molecular simulation-derived features for machine learning predictions of metal glass forming ability", Computational Materials Science 199 (2021) and has been adapted for use in this thesis.

3.1. Chapter Abstract

We have developed models of metallic alloy glass forming ability based on newly computationally accessible features obtained from molecular dynamics simulations. Since the discovery of metallic glasses, there have been efforts to predict glass forming ability (GFA) for new alloys. Effective evaluations of GFA have been obtained but generally relied on knowledge of alloy characteristic temperatures like the glass transition, crystallization, and liquidus temperatures but are of limited utility because these features require synthesizing and characterizing the alloy of interest. More recently, machine learning approaches to predict GFA have employed more accessible model features such as the elemental properties of constituent elements. However, these more accessible features generally provide less predictive accuracy than their less accessible counterparts. In this work we showed that it is possible to increase the predictive value of GFA models by using input features obtained from molecular dynamics simulations. Such features require only relatively straightforward and scalable simulations, making them significantly easier and less expensive to obtain than experimental measurements. We generated a database of molecular dynamics critical cooling rates along with associated

candidate features that are inspired from previous research on GFA. Out of the list of 9 proposed GFA features, we identify two as being the most important to performance through a LASSO model. Enthalpy of crystallization and icosahedral-like fraction at 100 K showed promise because they enable a significant improvement to model performance and because they are accessible to flexible ab initio quantum mechanical methods readily applicable to almost all systems. This advancement in computationally accessible features for machine learning predictions GFA will enable future models to more accurately predict new glass forming alloys.

3.2. Introduction

Since the discovery of the first melt quenched metallic glass in 1960, there has been a continuous search for new glassy alloys [35]. This search has yielded glassy alloys of scientific and commercial interest [5,14,15]. While successful, the rate of discovery of new alloys has been slow and only a small fraction of the possible search space has been explored [36]. The search for new glassy alloys can be broadly classified into two main methodologies. The first employs qualitative predictions of glass forming ability (GFA) using a variety of criteria such as searching for deep eutectics and identifying alloys with large atomic size mismatches [4]. The second methodology is focused on quantitative predictions of GFA which is measured by two main metrics: the critical casting diameter (D_C) or the related critical cooling rate (R_C). This study focuses on the second category of quantitative models, which give direct predictions of a GFA metric.

Quantitative models for GFA have taken different forms during their development and can be compared based on two factors: the accessibility of features used as inputs for

the model and the predictive value of the model. When looking at a typical materials discovery workflow, the accessibility of model inputs is important as it can define the size and scope of the search space that is available. The highest level of accessibility is for features of a target alloy that are known without requiring any significant computation or experiments. For example, recent machine learning based models that only rely on elemental properties of constituent elements use such highly accessible features [18,23,24,37]. At the lowest level of practical feature accessibility are properties that require synthesizing and experimentally characterizing properties of the target alloy in the glassy state (which we will simply call measured properties). Examples of these include various characteristic temperatures of a glass such as the glass transitions temperature (T_g), the crystallization temperature (T_x), and the liquidus temperature (T_l). While informative, these features are significantly harder to obtain and present challenges in a materials discovery workflow because of the necessity to synthesize a glass prior to evaluating its GFA. The predictive value of a model covers both the quality of predictions (domain and accuracy) of a model as well as what GFA metric a model is designed to predict. The two most direct and most common metrics of GFA are the critical casting diameter (D_C) and critical cooling rate (R_C). Both offer high value as they are direct measures of GFA. Another measure of GFA with lower predictive value is the ability of an alloy to form a glass under specific cooling conditions. For example, recent machine learning models to predict GFA have predicted a probability of forming a glass under melt spinning conditions, which can be very useful, but is not as direct a measure of GFA as a prediction of D_C or R_C [23].

Across this spectrum of input features and predictive value most models fall into two camps. They either use easily accessible features and sacrifice predictive value or they use features that are relatively inaccessible and can maximize predictive value. If more accessible features were available that maintained their information related to GFA, it would potentially be possible to generate machine learning models that have the best of both camps, *i.e.*, easy predictions that are highly accurate. The spectrum of models along these feature accessibility and prediction value metrics is summarized in *Figure 1.2*, and the goal of this work is to help develop models that are in the upper right quadrant. Models that fall in the bottom left quadrant would generally be uninteresting and not useful, and current models fall either in the top left or bottom right quadrants.

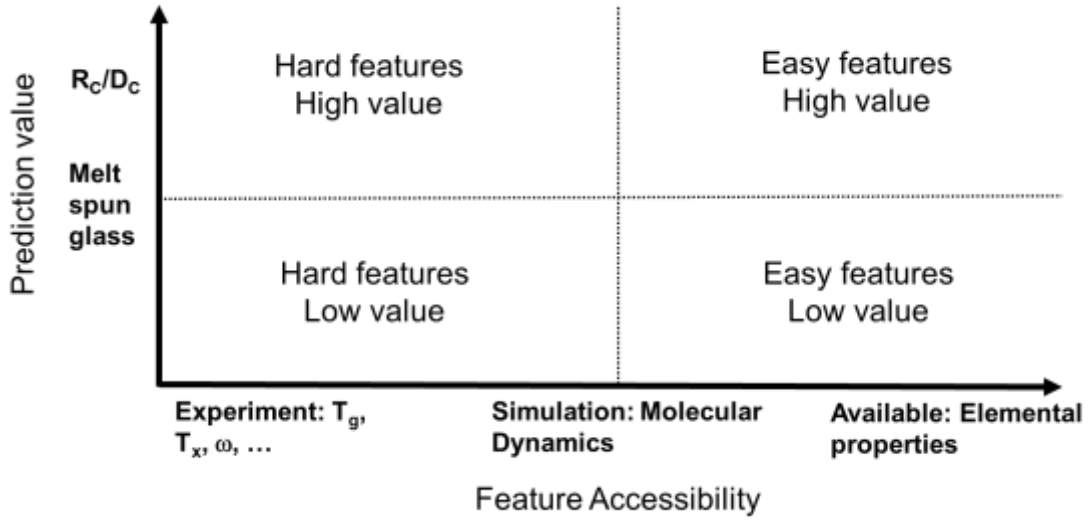

Figure 3.1. Outline of Feature Accessibility and Predictive Value Spectrum. (*Reproduced from Chapter 3*).

To find a middle ground in which predictive value is maintained while increasing feature accessibility, we used high throughput computational simulations to generate a range of features. These features are all generated by performing Molecular Dynamics

(MD) simulations to quench a variety of metal alloys to extract information from the quench run or the resulting amorphous structure. In an ideal world, we would be able to perform these simulations on alloys with experimentally measured GFA metrics to use as the training and testing data. However, the overlap between alloys with measured GFA metrics and available interatomic potentials is relatively small. Therefore, we calculated the R_C values directly from MD simulations by performing a series of quenches at varying cooling rates to obtain the GFA data for training and testing. This approach comes with a few limitations. Due to simulation time limitations, the accessible cooling rates are 109 K/s and above. This high value means that conclusions obtained here will be limited to low GFA alloys. However, the hope is that lessons learned in this range may give insight into GFA for higher GFA alloys as well. The second limitation is that available interatomic potentials are not necessarily fit to amorphous structures and may misrepresent them in some way. Because all the data calculated will be using the same types of potentials, the R_C values and features are at least fully self-consistent, although they may not match experimental values.

3.3. Methods

A computational critical cooling rate database was generated using the large-scale atomic/molecular massively parallel simulator (LAMMPS) molecular dynamics software found at http://lammps.sandia.gov [38]. The critical cooling rates were estimated by performing temperature ramps from 2500K to 100K in 50K steps. The hold time at each step was varied to achieve cooling rates ranging from 10^{14} K/s to 10^{11} K/s. Eleven binary systems were investigated: Al-Ag, Al-Cu, Al-La, Al-Sm, Al-Zr, Cu-Mg, Cu-Ni, Cu-Zr, Mg-

Y, Ni-Zr, and Pd-Si. These binaries were chosen from available binary EAM potentials due to overlap with existing known glass forming systems as well as to maximize variety of elements included[39]. For each binary system, compositions near the edges of the binary were simulated with a maximum of 10% of the minority element. This was done because we can only calculate R_C if it is within the cooling rate range given above, which corresponds to what are generally considered bad glass formers. Bad glass formers are expected to occur near pure elements. For each composition and cooling rate, 10 cooling runs were performed to account for the stochastic nature of crystallization during cooling. To find R_C we used the following approach. First, we identified the slowest cooling rate at which more than 50 percent of cooling runs amorphized, denoted R_C *(2)*, The cooling rate on sampling step slower than R_C *(2)* was denoted R_C *(1)*. We then assumed that the fraction of runs that yielded amorphous material was a linear function of R_C between R_C *(1)* and R_C *(2)* and solved for the cooling rate that gave exactly 50% of runs amorphizing. This was taken as R_C. From the compositions and cooling rates simulated, 78 critical cooling rates were found and used in a critical cooling rate database.

Ten highly accessible features are considered as inputs for machine learning models. The first nine (excluding the ELEM features discussed more below) are from simulations or could be obtained from simulations. These nine features will be referred to as the “GFA features” or “GFA feature set” going forward. The features are all inspired from previous research in modeling GFA. Some are directly taken from previous literature, and some are modified to fit into a high-throughput simulation workflow. A summary of the GFA and ELEM features can be found in *Table 3.1*.

Table 3.1. Summary of GFA features generated for machine learning models.

Feature	Source
1. glass transition temperature (T_g)	cooling
2. liquidus temperature (T_l)	phase diagram
3. reduced glass transition temperature (T_{rg})	previous features 1 and 2
4. atomic packing density (APD at 100K)	cooling
5. icosahedral-like (ICO-like) fraction (at 1.2 T_g)	1.2 T_g hold
6. icosahedral-like (ICO-like) fraction (at 100K)	cooling
7. diffusivity (at 1.2 T_g [D])	1.2 T_g hold
8. variance of Voronoi Polyhedra (Var)	cooling
9. enthalpy of crystallization	energy minimization
10. elemental features (ELEM)	MAST-ML

We obtained the glass transition temperature T_g from the 10^{14} K/s rate cooling run for all systems. T_g values obtained at this high cooling rate are known to have a significant shift from experimental glass transition temperatures which may limit usefulness of this computational T_g, but there may be useful information that can be extracted. Furthermore, getting an estimate of T_g is necessary for several of the other features which are defined in relation to T_g.

The liquidus temperature (T_l) is the second feature that has been used in some of the earliest models to predict GFA[40]. This feature was extracted from existing phase diagrams and not directly computed. While obtaining values in this way requires experiments at some point, they can be extrapolated from existing data so effectively that

we consider them to be highly accessible. The liquidus values could also be simulated with MD with reasonable fidelity if needed.

The reduced glass transition temperature ($T_{rg} = T_g / T_l$) is one of the oldest features used to predict GFA [40]. Using this simple combination of the previous two features, we can potentially learn if this ratio improves learning compared to the base features that compose it. If a highly complex machine learning model was generated, we might expect this relationship to be learned. However, because a simple model is being used, providing the relationship directly may improve the model.

The atomic packing density (APD) feature has been shown to affect the mechanical properties of metallic glasses and has been loosely been tied to GFA [41–43]. The APD is calculated from the resulting amorphous structure after the 75 K/ps cooling runs and is averaged over the 10 runs. Similar to other features, the final structure was taken after a final energy minimization of that resulting structure. Metallic atomic radii and empirical atomic radii where used for the APD calculations are taken from the pymatgen materials analysis library [44].

The Icosahedral-like (ICO-like) fraction has been used as a feature linked to glass forming ability in a variety of systems [45–48]. In this work, we calculated two variations of ICO-like fraction. The first was obtained at 1.2 times the T_g feature calculated previously. The second was taken from a snapshot of the final structure after cooling to 100K at the 75 K/ps cooling rate. In both cases, static energy minimization was performed in order to more clearly observe the underlying structure. In our definition of ICO-like fraction, we used the definition proposed by Bokas et al [42]. Icosahedral like clusters are identified based on Voronoi polyhedral indices of each atom and the ICO-like distinction

is a slightly broader inclusion than the pure <0,0,12,0> indices. The fraction is the sum of atoms classified as ICO-like divided by the total atoms in the simulation.

The diffusivity (D) feature is the average self-diffusivity of the atoms in the system, regardless of composition. It was found by performing an additional temperature hold at 1.2 T_g. This feature is different than previous features because it is not trying to mimic a feature directly suggested by previous research. Instead, D is calculated as a way to include a kinetic feature whereas many of the others included are structural. A multiple time origins approach was used to calculate self-diffusion using the Einstein relation on mean squared displacement [49,50].

The Variance of Voronoi Polyhedra (Var) is a feature recently explored by Wang et al. [20] as a way to analyze the liquid structure and gain information about GFA. The variance of cluster fractions is defined as:

$$\sigma^2 = \frac{\sum_i (X_i - \mu)^2}{N_c} \tag{3.1}$$

where X_i is the fractional contribution of a cluster type to the structure, μ is the average of the cluster fractions, and N_c is the number of cluster types included in the calculation. As N_c increases, cluster types with progressively lower fractions are included in the metric. This leads to a natural maximum in a plot of variance with respect to number of clusters included. In our work, this maximum variance is used as the variance metric as opposed to variance at a fixed number of clusters as was done by Wang et al. [20]. This modification was done because otherwise the metric varied widely from system

to system with respect to the number of polyhedral averaged making it impossible to select a specific converged value for N_c.

The Enthalpy of Crystallization ($\Delta H_{crystal}$) is a feature inspired by related investigations of the competition between crystalline and amorphous phases [37,51,52]. In previous work, enthalpies have been obtained experimentally. Here we calculated a simple approximation of the enthalpy difference by taking the difference between the final amorphous structure obtained after the 75 K/ps cooling runs and 3 candidate crystal structures. $\Delta H_{crystal}$ is then defined as the minimum enthalpy difference between the amorphous structure and the three crystals. The three crystal structures generated are BCC, HCP, and FCC solid solutions of the relevant composition. Elements are randomly assigned to lattice positions in the appropriate ratios and the lattice volume is relaxed while fixing atoms on their lattice sites.

The Elemental Feature (ELEM) set is a set of elemental features compiled by Ward et al. and has been shown to be useful in a variety of applications in predicting materials properties purely from compositional information [24]. We used this feature set in combination with the MAterials Simulation Toolkit – Machine Learning (MAST-ML) [53,54] to generate a list of compositional features that includes the composition average, arithmetic average, minimum, maximum, and difference of the elemental features. Thus, this feature entry in *Table 3.1* actually corresponds to a long list of features that require no simulations to generate.

One common GFA criteria that was not included is the onset of crystallization temperature (T_X) [17,55–58]. This feature has not been simulated for a few different reasons which make it impractical to obtain in high-throughput fashion. The first is that

T_X is known to be highly sensitive to the heating rate. Previous experimental investigations such as those by Zhuang et al. have shown that changes in heating rate from 5 K/s to 80 K/s can result in a change of around 20K in T_X [59]. The simulated heating rates, which if assumed to be on the same scale as the slowest cooling rates achieved in this work, would be eight orders of magnitude faster than those experiments and likely lead to large errors in T_X. In some cases one can extrapolate from computational time scales to experimental time scales through generating Time-Temperature-Transformation (TTT) curves from isothermal holds at multiple temperatures, such as those completed by Louzguine-Luzgin, and Bazlov [60]. However, this approach requires many simulations for each material, and the approach has only been demonstrated on pure elements Iron and Copper. For any alloys with better GFA it is expected that simulation time for these holds would increase dramatically. Because of these concerns T_X was not pursued as a feature in this work. However, in the future it may be possible to add this to the feature set explored here.

All the models built used the MAST-ML machine learning toolkit which uses sci-kit learn implementations, models, and analysis tools [53,54]. The following model types of varying complexities were investigated: LASSO, Ridge Regression (RR), Random Forest (RF), and Gaussian Kernel Ridge Regression (GKRR). For each model, the hyperparameters were optimized via grid search and the performance was estimated with 5-fold cross validation. Using the GFA feature set, all models gave 5-Fold root mean squared errors within observed variance due to random splitting of train and test splits. Therefore, one model was chosen to report results on in this investigation. The LASSO model was chosen for its simplicity and ease of interpretability. Two models were built.

The first model, referred to as the baseline model, uses only the ELEM set. The second model uses both ELEM and the range of GFA inspired features discussed above.

3.4. Results and Discussion

The results from training on the ELEM features model are shown in *Figure 3.2*. The parity plot shown is the average result from 20 individual 5-Fold cross validation splits and the error bars are the standard deviation of predictions across those 20 splits. The lack of correlation between the predictions and true values makes it immediately clear that the model does not perform well and has essentially no predictive value beyond getting the average value. The Root Mean Squared Error (RMSE) divided by the standard deviation in the training set (σ_y) value approaches one, demonstrating that errors in predictions are on the same scale as the spread in the training data.

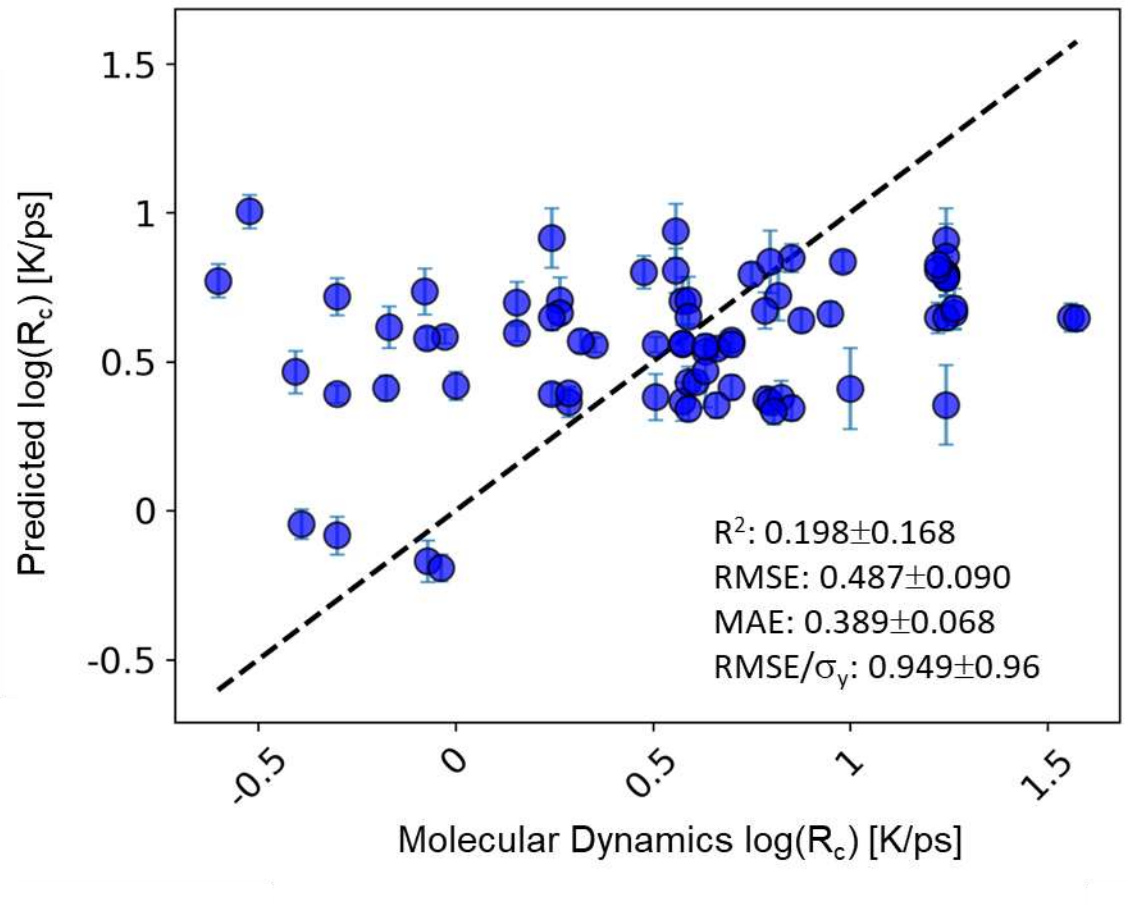

Figure 3.2. 5-Fold cross validation predictions of the baseline LASSO model. Error bars show the standard deviation in predictions over 20 cross validation runs. Error metrics are averages of individual statistics from each cross validation run.

Figure 3.3 shows the results of the model with the full feature set (ELEM and GFA features). Qualitatively, it is clear that the model has improved. The RMSE divided by σ_y has dropped considerably when compared to the elemental-only model. Now, the RMSE is about half of the spread in the data. The R^2 value has also increased to 0.77 from 0.20.

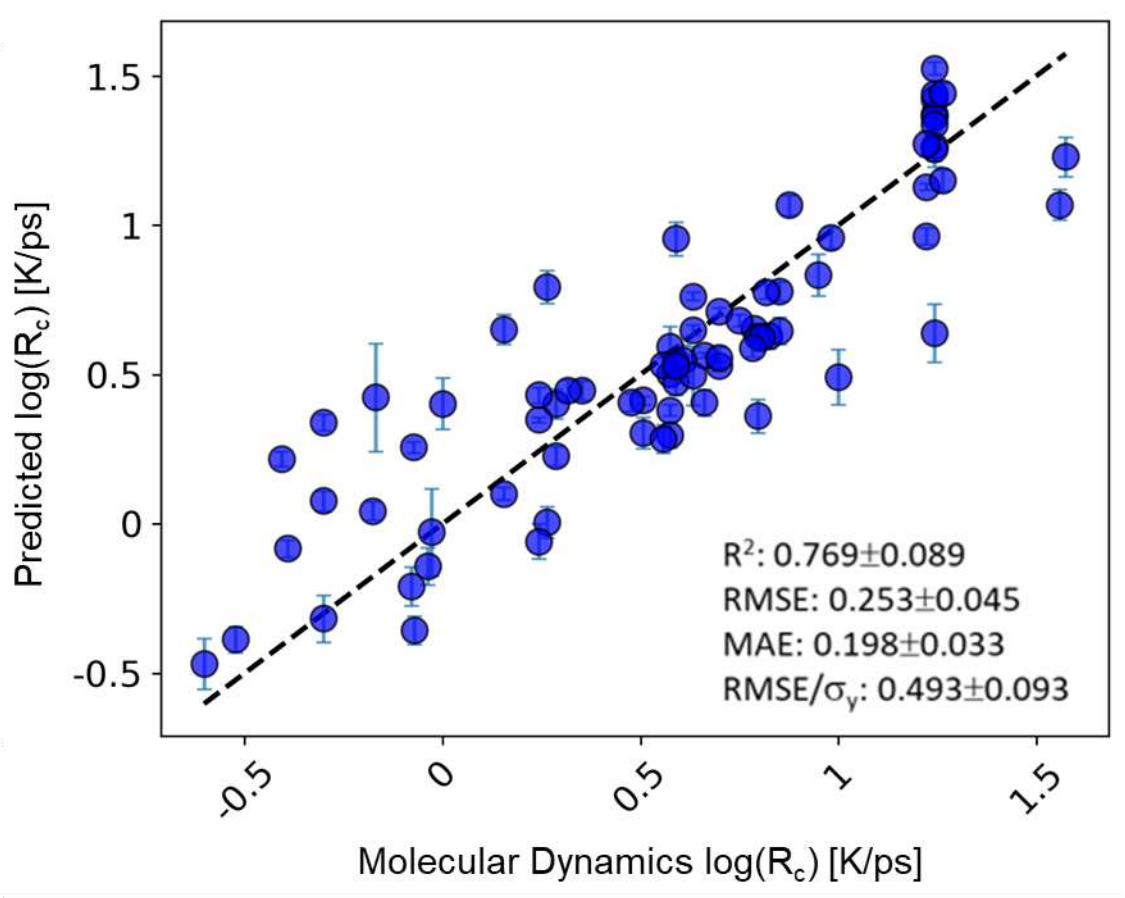

Figure 3.3. 5-Fold cross validation predictions of the model using the GFA feature set. Error bars show the standard deviation in predictions over 20 cross validation runs. Error metrics are averages of individual statistics from each cross validation run.

An addition to discussion of model performance we would also like to address several limitations with this model. The first is that it is important to note that the extremely high cooling rates accessible to MD simulations mean that the model only has access to training data on poor glass formers. Therefore, any predictions of good glass forming materials such as melt-spun glasses or bulk metallic glasses would be large extrapolations from the training data over multiples orders of magnitude in R_C. Due to the large extrapolation needed we expect any predictions of even moderately good glass formers would have large uncertainties associated with them. Furthermore, available

interatomic potentials limit access to a majority of good glass forming systems which would be of the most interest to predict and compare to known GFA metrics. One binary system where we do have access to interatomic potentials is the Cu-Zr binary. Predicting R_C for the $Cu_{50}Zr_{50}$ alloy gives an R_C value of 0.19 K/ps which is equivalent to -0.71 on the log scale in *Figure 3.3*. While this prediction in lower than all the training data range it is still about 13 orders of magnitude faster than the known R_C value of 250 K/s [61]. This result is expected and highlights that the focus of results for training this model is not in making significant new predictions but in learning which features were important for model performance within the model's training domain.

We explored which features contributed the most to the predictive improvement. During model training, no feature selection was performed ahead of model training. The fitting process of the LASSO model performs an internal feature selection and produced a total of 48 features with non-zero coefficients. Looking at the magnitude of coefficients obtained during model fitting, we determined that a small number of features played a dominant role in the performance of the model. The magnitude of coefficients for the ten most important features is shown in *Table 3.2*. Note that all features have been normalized to have a minimum value of 0 and a maximum value of 1 in order to directly compare coefficients. Within 10 features, the coefficient drops by almost an order of magnitude. As a quick test for significance of features, a model was generated using only these top 10 features and it showed a RMSE of 0.25 ± 0.04 which is essentially identical performance to the full model shown in *Figure 3.3*. Six out of the top ten features came from the GFA features, demonstrating that the additional GFA features are critical to the improved model performance.

Table 3.2. Magnitudes of LASSO coefficients for the top 5 features in the second model that used both elemental features as well as the calculated GFA features are tabulated.

Feature Name	LASSO Coefficient	Feature Class
enthalpy of crystallization	2.22	GFA
icosahedral-like (ICO-like) fraction (at 100K)	1.08	GFA
mendeleev number (Average)	0.93	ELEM
glass transition temperature (T_g)	0.44	GFA
diffusivity (at 1.2 T_g [D])	0.44	GFA
boiling temperature (average)	0.33	ELEM
APD (at 100K)	0.31	GFA
BCC crystal volume per atom (average)	0.31	ELEM
icosahedral-like (ICO-like) fraction (at 1.2 T_g)	0.29	GFA
number of unfilled valence orbitals (average)	0.28	ELEM

Figure 3.4 shows the four features with highest coefficients plotted against R_C. Qualitative differences between the effectiveness of the four features can be readily seen. First, the $\Delta H_{crystal}$ feature shows a significantly better relationship than the other three features, with an RMSE (R^2) of 0.36 (0.52). The Icosahedral-like Fraction also shows some significant correlation, with an RMSE (R^2) of 0.46 (0.22), but the Mendeleev Number and Tg show no simple linear correlation.

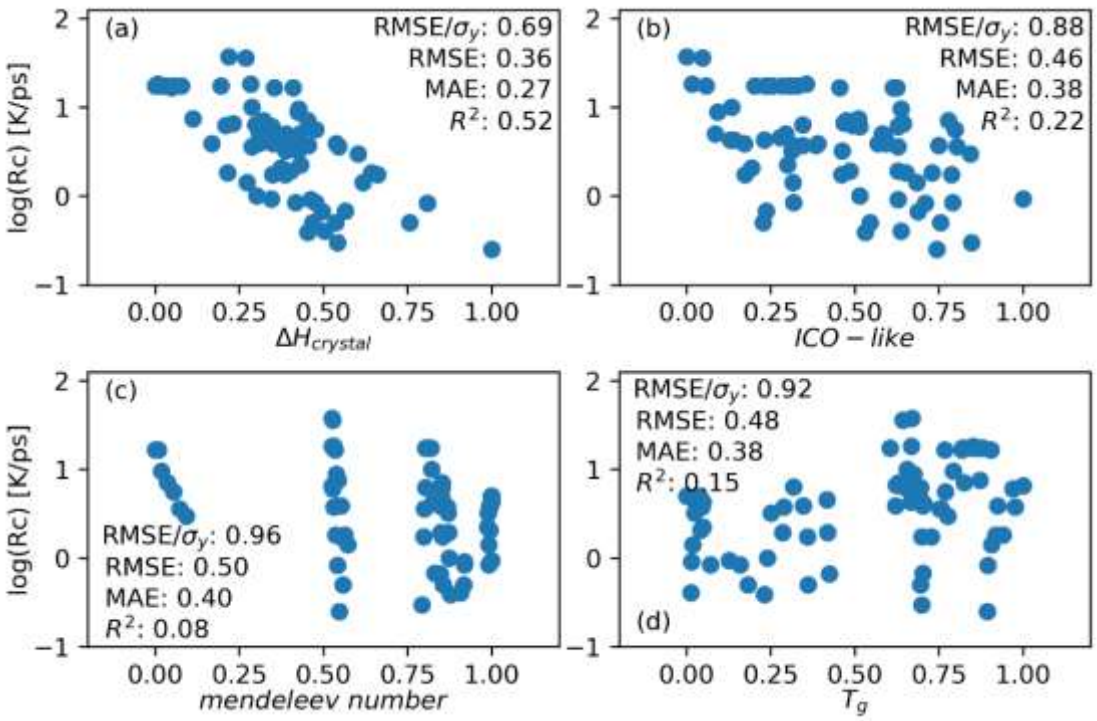

Figure 3.4. The top four features are plotted individually against the critical cooling rate. (a) Enthalpy of crystallization, (b) Icosahedral-like Fraction at 100K, (c) Mendeleev Number (average), (d) T_{rg}.

The two GFA features with the largest coefficients, the enthalpy of crystallization and the ICO-like fraction, are particularly interesting because they are quite easy to obtain computationally. Once a rapidly quenched structure is obtained, the ICO-like fraction feature can be directly calculated with minimal computational cost. The enthalpy of crystallization feature requires 3 extra calculations. However, each of these three calculations is a static energy minimization and not a computationally intensive molecular dynamics run. The accessibility of these two features means that both are practically obtainable via ab initio quantum mechanical methods and are not limited to simulations using interatomic potentials.

The enthalpy of crystallization is an estimate of the driving force for crystallization. Previous studies estimated this driving force using empirical and semi-empirical models

such as those by Miedema [51,52]. This work demonstrates how a computational analog to this driving force, directly comparing simulated enthalpies of rapidly quenched amorphous structure and a reference crystal, can capture key thermodynamic information about glass forming ability from a fairly simple and fast simulation.

The ICO-like fraction has been studied experimentally and with ab initio calculations and has recently been effectively correlated with trends in glass formation ability within the Al-Sm-X, Cu-Zr, Cu-Zr-Nb, Ce-Ga-Cu, and Ni-Nb systems [47,62–64]. These studies have typically been focused on single systems and correlating GFA trends within the system with this local structure feature. This work demonstrates how the ICO-like fraction gives structural information that correlates with trends in GFA between alloy systems and not only GFA within select systems.

3.5. Ab-initio enthalpy of crystallization

Note: This section is not included in the paper this chapter is adapted from.

One of the biggest limitations to the developed enthalpy of crystallization feature in this chapter is its inherent reliance on the EAM potentials used to calculate it. While these potentials are fast and can enable the kinds of high throughput simulations performed, they also come with the downside that they need to be fit specifically for each alloy that needs to be investigated. This fitting process requires significantly more time than any of the other steps in the model training and predictions process and would quickly become the rate limiting step in any approach to use these features as is. Therefore, there is significant motivation to develop the features further so that they rely less on steps that require time consuming human interaction.

An initial study was performed to transfer the enthalpy of crystallization feature from classical MD to ab-initio MD. For 53 alloys with measured R_C values the enthalpy of crystallization feature was simulated using the Vienna ab initio Simulation Package (VASP) [65]. Ab-initio methods have a significant benefit in that the pseudopotentials that describe the simulated atoms and electrons do not need to be refit for every new alloy, entirely removing any limitation to transitions between alloys. However, they were not pursued originally due to limitations in computational speed. In order to generate the full quench simulation to a similar amorphous structure to the classical MD simulation the simulation size had to be reduced from 19,000 atoms to 1,000 atoms. Furthermore, the quench rate and temperature step had to be increased from 50K to 200K. This enabled us to obtain an amorphous structure from the quench, however these changes may have had significant effects on the resulting structure.

The direct relationship of the calculated enthalpies with experimental R_C values is shown in *Figure 3.5* Overall it still seems like there may be some relationship there, however quantitative metrics have dropped noticeably compared to *Figure 3.4*. Specifically, RMSE and MAE have increased by almost an order of magnitude. In contrast the R^2 and RMSE/σ_y values have remained fairly constant due to the significant increase in the range of experimental R_C values compared to the computational database.

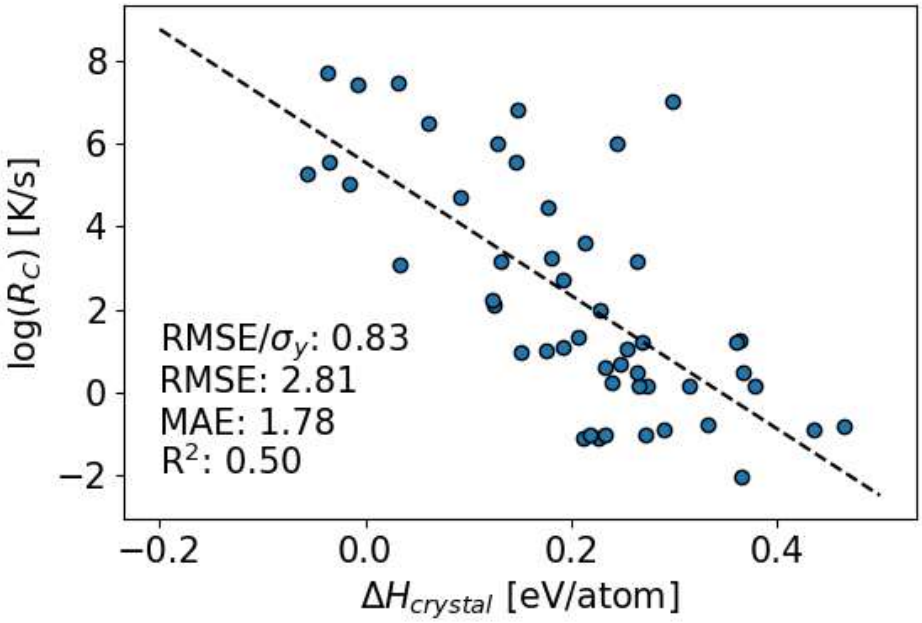

Figure 3.5. Ab-initio enthalpy compared to experimental R_C values. RMSE/σ_y is 0.83, RMSE is 2.81, MAE is 1.78, and R^2 is 0.50.

To replicate the previous results from section 3.4 two more LASSO models were trained and assessed using 5-fold CV. *Figure 3.6* shows the results of the baseline set of elemental property features. Compared to the previous models the elemental property features are capturing more information about the R_C though the error metrics of R^2 = 0.58, RMSE = 1.93, MAE = 1.21, and RMSE/σ_y = 0.713 combined with qualitative observations of the very large outliers in poor predictions mean this model is still not predating R_C well. This holds true for *Figure 3.7* as well, which shows results for a LASSO model trained with both the elemental property features and the enthalpy of crystallization feature. Key error metrics are R^2 = 0.59, RMSE = 2.01, MAE = 1.28, and RMSE/σ_y = 0.732.

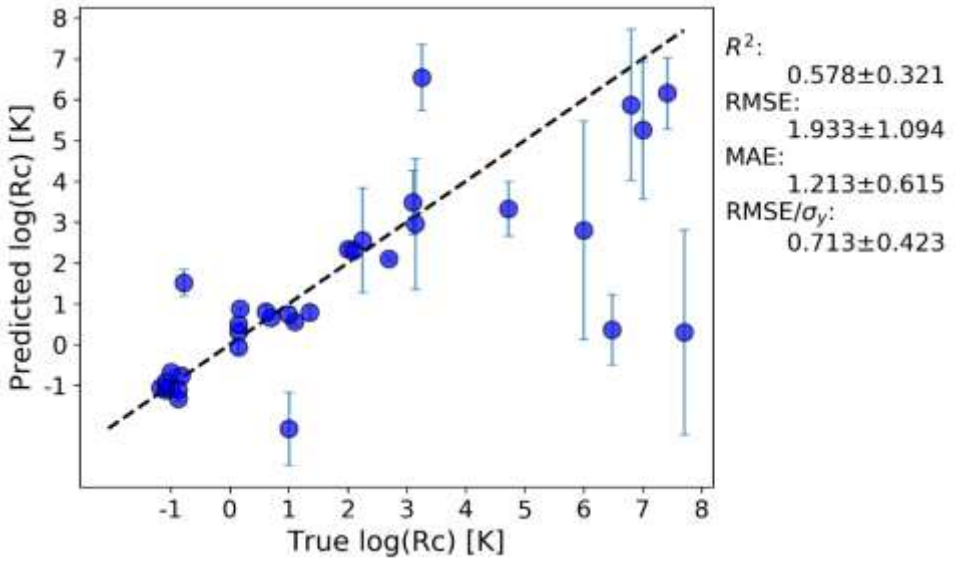

Figure 3.6. 5-Fold cross validation predictions of the baseline LASSO model. Error bars show the standard deviation in predictions over 20 cross validation runs. Error metrics are averages of individual statistics from each cross validation run.

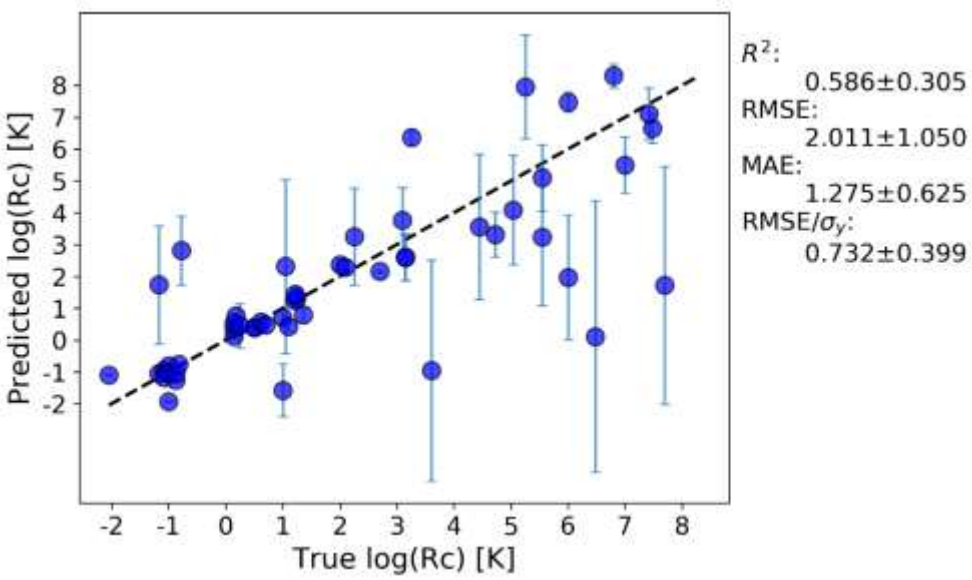

Figure 3.7. 5-Fold cross validation predictions of the LASSO model with ab-initio enthalpy feature. Error bars show the standard deviation in predictions over 20 cross

validation runs. Error metrics are averages of individual statistics from each cross validation run.

This initial study to transfer the enthalpy of crystallization feature to ab-initio methods did not yield promising results. However, there are several causes for the lack of performance. First, the significant compromises to the quench and simulation size discussed before. Furthermore, it's important to note that the enthalpy feature also relies on an accurate estimate of the competing crystal reference state in its calculation. Similar to the previous work in this chapter crystal references were approximated as solid solutions of FCC, BCC, and HCP crystals. While this may have worked well when the previously compositions were all close to the boundaries of the composition (<10% minor alloying element), many of these alloys were in the center of the composition range meaning competing crystals are likely intermetallic compounds. Future development to calculate more accurate crystal reference states may be necessary before the enthalpy of crystallization feature can be accurately simulated.

3.6. Conclusions

Using a simulated database of Rc, we demonstrated how computationally generated features inspired by previous GFA research can be used to improve a model's ability to predict Rc of an alloy. It was found that enthalpy of crystallization and ICO-like fraction contributed most to the improved performance of the model. Both features can be practically extracted from ab initio quantum mechanical simulations, allowing them to be applied to a wide range of materials. We believe that using these simulated features in future models for GFA could significantly increase their accuracy while allowing for

readily obtainable input features. We are pursuing such studies now to build on the present work.

Chapter 4. Synthesis of Datasets for Predicting Critical Cooling Rates

Note: This chapter has been submitted for peer-reviewed publication in Nature Communications and has been adapted for use in this thesis.

4.1. Chapter Abstract

We use a random forest model to predict the critical cooling rate (R_C) for glass formation of various alloys from features of their constituent elements. The random forest model was trained on a database that integrates multiple sources of direct and indirect R_C data for metallic glasses to expand the directly measured R_C database of less than 100 values to a training set of over 2,000 values. The model error on 5-fold cross validation is 0.66 orders of magnitude in K/s. The error on leave out one group cross validation on alloy system groups is 0.59 log units in K/s when the target alloy constituents appear more than 500 times in training data. Using this model, we make predictions for the set of compositions with melt-spun glasses in the database, and for the full set of quaternary alloys that have constituents which appear more than 500 times in training data. These predictions identify a number of potential new bulk metallic glass (BMG) systems for future study, but the model is most useful for identification of alloy systems likely to contain good glass formers, rather than detailed discovery of bulk glass composition regions within known glassy systems.

4.2. Introduction

Bulk metallic glasses (BMGs) are a class of materials with exceptional properties that support a wide range of application spaces including biomaterials, magnetic devices, and in surface coatings [14,15]. A key challenge in BMG materials discovery is identification of BMG forming compositions in existing glassy alloys and discovery of entirely new BMG alloys. Methods for discovery of BMGs have generally fallen into two broad categories. The first category is qualitative predictions of good glass forming ability (GFA) alloys and regions through identification of various qualitative and semi-quantitative physics-based criteria (e.g., deep eutectics) such as those outlined by Inoue et al [4]. This methodology has had many successes and is responsible for the discovery of many of the BMG alloys known today. The second category is models that quantitatively predict a metric of GFA such as the critical cooling rate (R_C) or the critical casting diameter (D_c). As our understanding of glassy alloys, and the amount of available data increases, these quantitative models are becoming more appealing as they can potentially reveal much more detailed information about the GFA across alloys.

Quantitative GFA predictions take many forms but can be organized by their choices of features, models, and target predictions. Features typically range from approximately instantly accessible (e.g., elemental properties [18]) to moderately accessible properties needing some calculation (e.g., thermodynamic properties determined from CALPHAD [19], or liquid properties determined by molecular dynamics [20]) to properties requiring extensive synthesis and characterization (e.g., glass transition temperature [17,22,66] or fragility [21]). Models range from simple linear functions (e.g., the R_C vs. Ω correlations [17]) to fully non-linear machine learning models

(e.g., D_c vs features fit with boosted trees [22]). Target values range from qualitative categorical predictions (e.g., is a glass under melt spinning [23,67,68]) to quantitative models of R_C [17] and D_c [22,24,69,70]. A comprehensive review is not practical here, so we focus on the present status of efforts most similar to ours, where the focus is on instantly accessible elemental property features and quantitative prediction of R_C or D_c. We are not presently aware of any study that has successfully built a demonstrably effective predictive model for new BMG systems from simple elemental features. A few notable successes have been the work of Ren et al. and Ward et al., demonstrating a significant ability to predict categorical results of glass forming under melt-spinning, and optimizing GFA of existing known glass formers [24,71]. They fit to over 6,000 melt spinning experiments and achieved a AUC of 0.80 in their ROC curve [71]. Zhang et al. propose a combination of these ideas, using a two-step approach to layer classification predictions with subsequent D_C predictions from a similarly accessible feature set [72]. These works show the power of elemental property features but do not provide an approach to predict new BMG systems. In terms of predicting R_C and D_C there have been striking successes for R_C predictions from characteristic temperatures (liquidus, glass transition, and crystallization temperatures), with Long, et al. reporting an R^2 of 0.93 vs. the Ω parameter, which is a simple function of characteristic temperatures [17]. D_C has generally been harder to predict quantitatively [17] although Johnson et al. [21] showed an outstanding result R^2 value of 0.98 in their predictions for D_c as a linear function of reduced glass transition temperature and fragility. These results suggest R_C is easier to model than D_C. These results also suggest that quantitative models of R_C and D_C are possible, although they have only been achieved by using very expensive features that require extensive synthesis and characterization for every new system. However, the

above work also suggests that elemental properties can capture physics of GFA, particularly when combined with the ability of modern machine learning methods to model nonlinear relationships and automatically select features. Taken together these observations raise the tantalizing possibility that an accurate model of R_C as a function of elemental features might be achievable.

The absence of a model relating R_C to elemental properties is easily understood as a result of the lack of adequate training data. There are approximately 10^2 R_C values from direct experimental measurements available. In addition, researcher interest in BMGs and limitations on measuring R_C (typically below 10^4 K/s) means most data is focused on alloys with known BMGs compositions, and often within composition ranges associated with the BMG formation. A machine learning model that is trained solely on this data will be heavily biased towards predicting that everything is a BMG, limiting the model's utility in identifying new BMG alloys. Limited and biased data are two critical issues holding back machine learning predictions of R_C from simple features like elemental properties. Similar arguments hold for D_c, although there are closer to 1,000 data points available [73].

Here we try to develop the first model for R_C as function of elemental features, with a focus on expanding the database of R_C from its directly measured values, as this database is too small to support robust machine learning models. This expansion is accomplished in three steps. First, available D_c data is converted to approximate R_C values using curve fitting to a functional form inspired by simple assumptions about heat transfer during cooling and average thermodynamic properties of metals. Second, available characteristic temperature data is used in combination with previously

developed models to estimate R_C for a range of alloys. And third, available melt spinning data is assigned approximate values for R_C. The goals of adding these different set of data are to provide more varied compositional space, increase the amount of training data, and expand the range of R_C values available for training. These methods expanded the amount of training data available by over an order of magnitude compared to direct measurements of R_C. Using this new dataset, a random forest (RF) model has been trained and evaluated for accuracy in predicting R_C and has also been used to predict the GFA in new BMG systems.

4.3. Methods

The starting R_C database was obtained primarily from Long et al. who gathered 53 experimental measurements of critical cooling rate [17]. One data point (pure nickel) was removed from this database due to being approximated by different methods. 25 more R_C measurements not in Long et al.'s database were found from eight more papers for a total of 77 experimental R_C measurements [74–81]. R_C values are converted to a log scale for easier representation across the wide range of orders of magnitude. Values range from 10^{-2} to $10^{7.7}$ K/s with an average of $10^{1.96}$ K/s. We will call this data set 1 (DS1).

DS1 was expanded three ways. First, we estimated R_C from experimental measurements of critical sizes from casting. We have used measurements of both critical casting diameter D_C and critical casting thickness Z_C, and we denote both as D_C. Both of these values are converted to R_C values using a generalization of the formalism outlined by Johnson et al. [82] which suggests the relationship

$$R_C = \frac{A}{{D_C}^B}. \qquad (4.1)$$

Johnson et al.'s proposed equation sets A=10 and B=2 based on assumptions about average thermodynamic properties across all metals. A fit of log(R_C) vs. log(D_C) (*Figure 4.1*) gives A=631 (log(A)=2.8), B=1.8. This fit was used to approximate R_C values from all D_C and Z_C values without a R_C in DS1. The A and B values shift quite significantly from the values estimated by Johnson et al. This difference is likely due to the previous assumptions ignoring surface interactions between the melt and the mold during casting. The application of Eqn. 4.1 in this first method added 342 approximate R_C values (which we call Data Set 2 (DS2)) and brings the number of training values up from 77 experimental R_C values to a total of 419 training values.

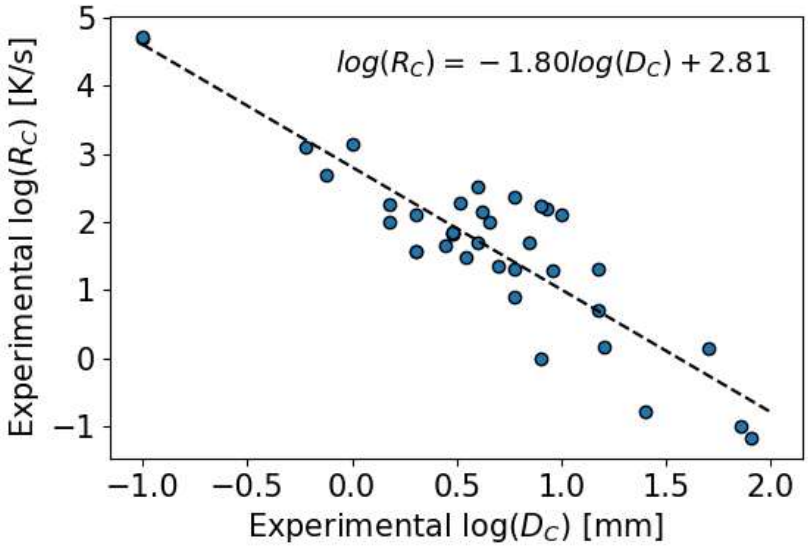

Figure 4.1. Comparison of a subset of training data with both experimentally measured RC and Dc values. The line of best fit and its equation are shown. The fit has R2 of 0.80, RMSE of 0.55 K/s, and MAE of 0.44 K/s.

Second, we used the ω parameter proposed by Long et al to make approximations for R_C for all datapoint for which we have measured T_g, T_X, and T_l [17]. Specifically, we take all T_g, T_X, and T_l data we have available, determine ω, and then use the linear relationship between ω and R_C to from Long et al to predict R_C. As an additional verification of the ω parameter, for the 25 additional points added to Long et al.'s original data, their ω values were calculated and are shown in the supplementary information as a test set specifically for the ω relationship. All the new values fell within the spread of the previous data, further demonstrating the ability of this parameter to effectively transform characteristic temperatures into estimated critical cooling rate values. Refitting the ω relationship proposed by Long, et al. only resulted in minor changes so to avoid a proliferation of almost identical models we simply used the fitting parameters established by Long et al. This second method added 141 approximate R_C values (which we call Data

Set 3 (DS3)) for compositions that do not overlap with previous datapoints, bringing the total to 560 compositions with approximate R_C values.

Finally, we leveraged melt spinning experiments, which categorize compositions as amorphous, partially amorphous, and crystalline under high-rate cooling. Based on what is known about typical cooling rates during melt spinning, these categories correspond to approximate constraints on R_C. Due to the overlap of the expected R_C values for amorphous melt spinning data (such alloys likely have R_C < ~10^5 K/s) with significantly higher quality measurements and approximations of R_C from the previous methods, the amorphous category data was excluded from the final dataset. This exclusion is done because introducing such a high amount of very approximate data in the range where we have much higher quality data would likely drown out any signal from experimental BMG values. We therefore assigned approximate R_C values only to the partially amorphous and crystalline categories and included them in our fitting. Specifically, we assigned the partially amorphous and crystalline cases R_C values of $10^{5.5}$ and 10^7 K/s, respectively. When a cooled system comes out partially amorphous it is likely that the actual cooling rate was a little slower than R_c since some of the system had time to crystallize. Furthermore, the cooling rate for melt spinning is known to be in the range 10^4 and 10^6 K/s, or based on averaging the logs, about 10^5 K/s. Therefore, for systems that are partially amorphous it is likely that the true R_c range is somewhat shifted toward higher values than the range 10^4 and 10^6 K/s, say $10^{4.5}$ and $10^{6.5}$ K/s. We represent this range by averaging the logs to give $10^{5.5}$ K/s. The value of 10^7 K/s for the fully crystalline was chosen to be a about one order of magnitude above the fastest cooling rate likely obtained in melt-spinning data to represent the fact none of these alloys formed

amorphous structures. The exact R_c value chosen for the crystal forming alloys did not have a significant effect on machine learning performance as we have an extremely small amount of direct experimentally measured R_C values in this range that would be affected by the specific number assigned to this data. Therefore, the main effect of including it and assigning a value is to allow the model to differentiate between the better glass formers found elsewhere in the dataset, and these poor glass formers.

The melt-spinning data is obtained from a review paper which provides over 8,000 melt-spun compositions[83]. From this dataset we used 1248 compositions which formed crystalline metals after melt-spinning, and 720 compositions which were categorized as partially amorphous. Although the R_C values from this data are highly approximate, they are quite distinct from the bulk of the higher-fidelity training data developed above and are therefore expected to constrain the fits without polluting fitting to higher fidelity data. *Figure 4.2* shows that the crystalline and partially amorphous data do not overlap significantly with the rest of the training data. This process added 1,565 approximate R_C values (which we call Data Set 4 (DS4)) for compositions that do not overlap with previous datapoints, bringing the total to 2,125 compositions with approximate R_C values. This is an increase of almost 30 times greater than the initial set of measured R_C values. We call this final integrated Data Set 5 (DS5).

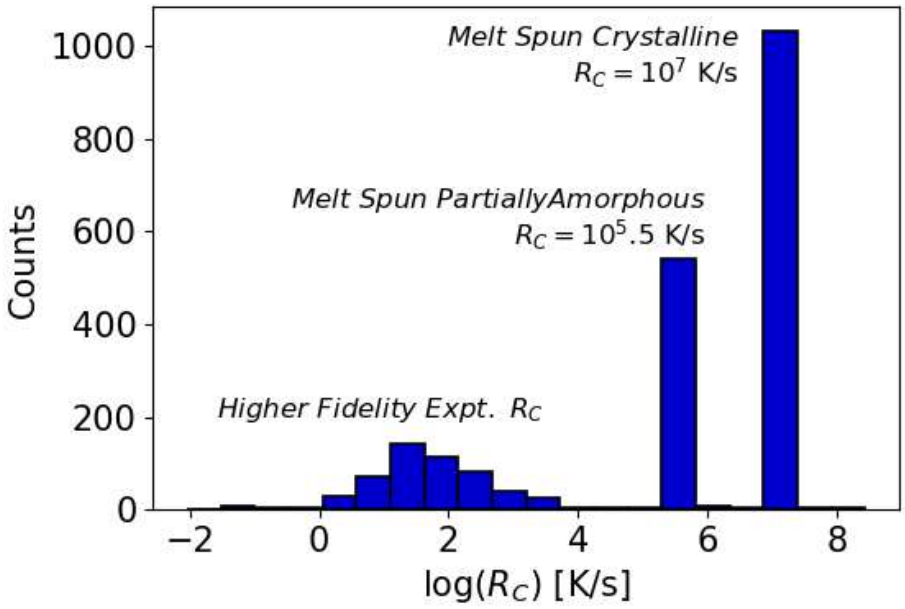

Figure 4.2. Distribution of R_C values in final training dataset (DS5)

Using the complete DS5 of R_C data a random forest model was built and trained to predict R_C. The random forest model is trained using the MAST-ML machine learning software package which builds machine learning workflows using the underlying scikit-learn python package [53,84]. Inputs to the model are obtained from compositional information and elemental features using the MAGPIE approach proposed by Ward et al. [18,24]. Elemental features for each composition are generated as composition averages, maximum, minimum, and difference. This feature set is chosen to be maximally accessible as all the features can be generated almost instantaneously directly from available elemental databases. Several other model types were also investigated along with the random forest model but showed worse performance. Specifically, gradient boosted trees and Kernel Ridge Regression models showed reduced performance under cross validation testing with a 5-fold cross validated RMSE of 0.732 and 0.803, respectively (compared to 0.36 for random forest, discussed below). We assessed the

predictive ability of the model through random and leave-one-group-out cross validation (CV). The random cross validation was done by repeating 5-fold cross validation 10 times (for a total for 50 left folds of data) and the predicted values for each excluded point were averaged.

4.4. Results and Discussion

The average predicted vs. true values are shown in the parity plot in *Figure 4.3*. We calculated the following statistics from the 5-fold CV test: $R^2 = 0.97 \pm 0.01$, root mean squared error (RMSE) = 0.36 ± 0.09, mean absolute error (MAE) = 0.08 ± 0.02, RMSE normalized by the standard deviation of all the $\log(R_C)$ values (RMSE/σ_y where $\sigma_y = 2.22$) = 0.16 ± 0.04 respectively. The error bars represent the standard error in the mean of each statistic when averaged over all 50 CV folds. Although our model uses only elemental features, the errors are comparable to or better than the best previous models for R_C using characteristic temperatures. Specifically, the ω model for predicting R_C from characteristic temperatures given in Long, et al. showed $R^2 = 0.90$ and RMSE = 0.67 log units [17]. These statistics are influenced by the large amount of melt spinning data which is somewhat unusual due to it being assigned the same R_C value. If the melt spinning data is excluded from the statistics RMSE value increases to 0.70 which is still essentially equivalent to the best previous characteristic temperature based models.

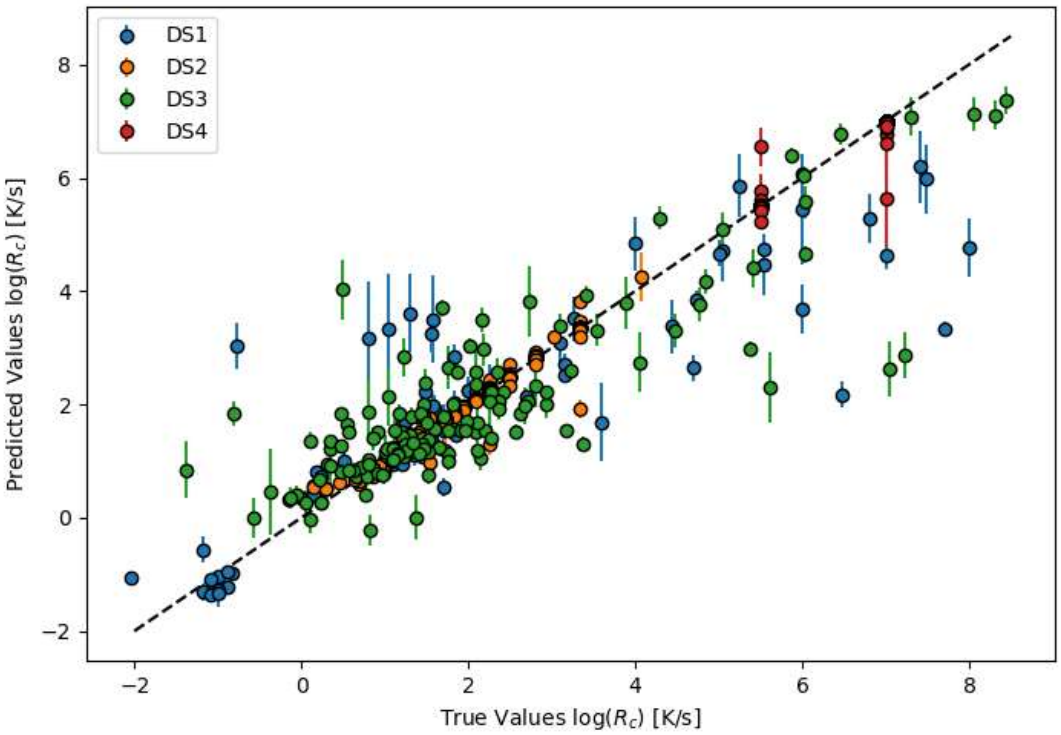

Figure 4.3. 5-fold cross validation performance of random forest model

While the random CV is a useful standard test of model accuracy it is not a good test of the ability of the model to predict new chemistries. This limitation of the random CV score arises because the data set often has multiple entries on closely related compositions due to the nature of experimental research on GFA, so excluded points in the validation data are likely to have similar compositions in the training data. The random CV score therefore likely overestimates how well the model will perform on new chemistries.

To assess errors on new chemistries we performed a leave-out-one-group CV, where we grouped together similar compositions and left them out one by one, training on the remaining data. Groups were defined by each unique alloy system. As each group was left out the training data the average RMSE were recorded and are summarized in

Figure 4.4. Groups are sorted by the minimum number of overlap instances with the training data between all elements in the group. For example, the elemental overlaps for an excluded Cu-Zr alloy would be the lower value between the number of Cu and Zr containing alloys were left in the training set. The dashed-dotted lines show the average RMSE of all groups within each bin from 0-250, and 250-821 on the x-axis. The dashed line shows the average across all points.

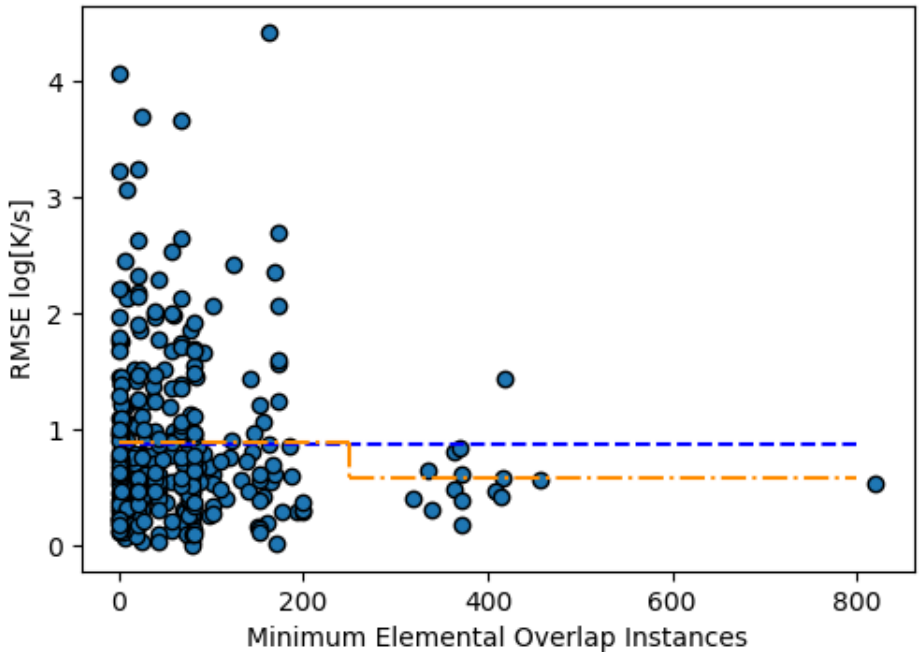

Figure 4.4. Leave out group cross validation sorted by amount of overlap with training data. The blue dashed line shows the average RMSE of 0.88 log units. The orange dashed-dotted line shows averages for each bin of data from 0-250 (0.89) and 250-821 (0.58).

Figure 4.4 shows how the model is performing on average and how it performs when there are many or few representatives of the elements being predicted. The average RMSE (MAE) of 0.88 (0.82) log units is noticeably larger than the random CV RMSE

(MAE) of 0.36 (0.08) log units. This increase is due to the larger amount of compositionally similar data being left out when an entire alloy system is removed. Due do the nature of experimental data generation many systems have measurements taken single digit atomic percents away from each other, which may cause the random CV method to overestimate performance. RMSE (MAE) errors still stay below an order of magnitude (one log unit) suggesting that in an average way the model is at least moderately robust to leaving out significant chemical information. One might expect that the model will perform best when there is the most training data. This effect is not particularly apparent from *Figure 4.4* but the data does seem to cluster into two groups, below about 250 and above, and the RSME goes from 0.89 to 0.58 in going from the low to high group. This result suggests that establishing a cutoff of around 250 elemental overall instances for elements in any predicted alloy systems may help improve the reliability of predictions.

Using the cutoff of 250 instances of overlap we can propose two searches for making predictions with the random forest model to identify new BMG systems. The first search is to use the model to predict likely BMGs from known glass formers from melt-spinning data. As discussed during the database generation section there is a set of melt-spinning data that was left out of model training due to overlap with the higher fidelity experimental data. We will look for BMGs within this group of alloys. We define a BMG as $R_C < 10^3$ K/s. This data has 3,755 compositions that were classified as glass formers under melt-spinning conditions. Of those points there were 63 compositions predicted as $R_C < 10^3$ K/s by our model and therefore predicted to be good BMG candidates. These predictions are shown in *Figure 4.5*. Predicted critical cooling rates of melt-spun glasses.

Points are color coded by interest of the alloy composition. Red points being the least interesting, and yellow points being the more promising as new BMG systems. with more details on the specific alloy systems given in *Table 4.1*. The probability of the prediction being a BMG is estimated directly from the random forest confidence interval of each prediction using a one-sided Z-test. An analysis of these estimated confidence intervals is included in the supplementary information in the section Error Bar Analysis.

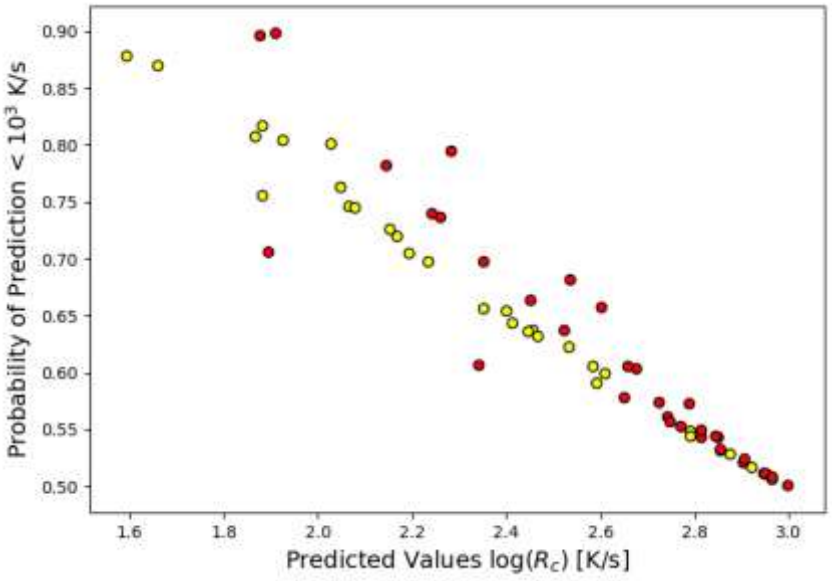

Figure 4.5. Predicted critical cooling rates of melt-spun glasses. Points are color coded by interest of the alloy composition. Red points being the least interesting, and yellow points being the more promising as new BMG systems.

While the machine learning model can potentially provide helpful guidance in discovering new BMGs, its predictions must be considered by human researchers to assess their value to the community. With this in mind, each prediction in *Figure 4.5* is color coded based on our personal assessment of the novelty of the alloy system for the BMG community. The color scheme is used in *Table 4.1* as well. Red systems are likely

the least interesting due to being a known BMG system in our training data. These predictions only demonstrate that the model will predict nearby compositions to training data. Yellow systems are not directly known BMG systems; however, they have nearby BMG quaternaries or ternaries with one additional minor alloying element. This limits the novelty of these predictions since we would expect the higher component systems to have better glass forming ability than the predicted lower component alloys. One of these systems, Al-Ca-Ga, is slightly different in that its nearby system is the binary Al-Ca system that is also included in *Table 4.1* which has less components. Of the yellow systems, Al-Ca-Ga is therefore the most potentially interesting as following the same logic this higher number of components in general may increase GFA compared to the known Al-Ca BMG system. Finally, there are several green systems that are potentially the most interesting due to not having any nearby known ternary or quaternary BMG systems. They can all be broadly grouped into the category of Au-B-rare earth. Predictions for these systems fell slightly above the previously established 10^3 K/s cutoff and are identified with an asterisk. This extension to higher R_C values was considered because previous established estimated errors in predictions still place these systems in the range of being potential glass formers. Based on our literature review this combination of elements appears to be new, with some of the closest systems being the Au-Si-X BMG systems introduced by Schroers et al.[85]. Our predicted alloys essentially replace the Si in the Au-Si-X BMG with another nearby metalloid, B. However, while rare earth elements have been used in BMGs there is not any previous literature combining gold and boron with rare earth elements of which we are aware. Therefore, these types of systems are suspected to be novel and worth additional consideration. As an additional check for potential interest in these systems we consider to what extent they are consistent with previously established empirical rules for

finding metallic alloys with high glass forming ability. While these criteria have many forms the following properties of systems proposed by Inoue et al. [12] are generally desirable: (1) multicomponent alloy consisting of more than 3 elements, (2) significantly different size mismatch exceeding 12% among the main 3 constituent elements, (3) negative heats of mixing among their main elements. We also add to this a fourth criteria, which is generally harder to assess without detailed thermodynamics models, which is that the system shows deep eutectics. All alloys are ternaries so do not quite satisfy the first criteria, but we know that BMG ternaries can be formed. All three systems easily satisfy the second criterion due to the large size difference between Boron and the Rare-earth elements. All three systems also satisfy the third criteria. Heats of mixing are calculated for each predicted composition from an extended regular solution model following the methodology and binary interactions from Takeuchi and Inoue [86]. Mismatch percentage along with the estimated heats of mixing, are shown in in *Table 4.1* for the average of predicted compositions in each system. With respect to the fourth criteria, available binary phase diagrams from the ASM Alloy Phase Diagrams Database were analyzed which reveal eutectics in all of the binary subcomponents of the Au-B-X ternary alloys [87]. Specifically, eutectics occur near $Au_{20}B_{80}$, near the edges of the B-X binaries as well as $B_{70}Gd_{30}$, and at many compositions in the Au-X binaries. While we do not have access to full ternary phase diagrams to investigate in more detail, agreement with many previously established criteria for discovery of BMG alloys makes these three systems interesting candidates for further study.

Table 4.1. List of alloy systems predicted as BMGs. Systems are color coded by potential to be novel BMG (see discussion in text for color coding).

Alloy System	Known BMG	Size Mismatch	Mixing Enthalpy (Kj/mol)
Cu Hf Nb	No	22%	-10.1
Cu Nb Zr	No	23%	-14.3
Cu Ti Zr	Yes	23%	-16.6
Ni Zr	Yes	26%	-44.8
Al Ca	Yes	39%	-18.0
Au B Pr*	No	131%	-63.2
Cu Hf	No	22%	-15.9
Al Ca Mg	Yes	39%	-14.0
Al Co Zr	Yes	25%	-46.0
Au B Er*	No	119%	-64.6
Au B Gd*	No	125%	-64.0
Cu P Zr	No	32%	-27.4
Al Ca Ga	No	39%	-22.9

To give more insight into the model's predictions, the R_C for systems in *Table 4.1* were predicted over the alloy's full binary and ternary composition ranges and the full predictions for the Au-B-Pr system are shown as an example in *Figure 4.6*. We can see from this example that a large portion of the ternary system is predicted near or below the 10^3 K/s cutoff for predicted bulk formation. This result, combined with the small dynamic range of predictions, with the majority of the ternary predicted within one order of magnitude, suggests we cannot claim to make a prediction of any specific region within the ternary being the most promising. This trend holds across most new predictions, suggesting that for new systems the model predictions can at best identify candidate BMG systems, rather than pinpoint promising BMG regions within systems. This limitation is unfortunate but may be less problematic in the future as the community is developing

new combinatorial approaches to experimentally investigate large composition ranges of a system. For example, researchers were recently able to synthesis and characterize R_C over a large region of the Al-Ge-Ni ternary using high-throughput methods [81].

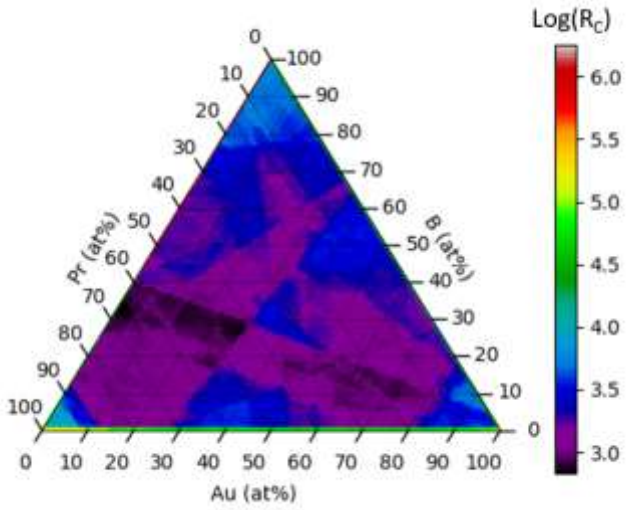

Figure 4.6. Predictions in 1% composition increments of the Au-B-Pr system.

A second search was performed to explore more widely for potential BMG systems. In the first test above potential systems and compositions were obtained only from known melt-spinning glasses. In this second test we considered every possible quaternary system composed of elements that meet the criterion of more than 250 overlap instances with the training set. There are 10 elements that meet this criterion in the training set: Al, Cu, Ni, Fe, B, Zr, Si, Co, Mg, and Ti. Making every single potential quaternary gave 286 potential quaternary systems. In each system a 10% composition grid was generated for the initial set of predictions. Due to the large number of predictions made multiple steps were taken to filter the predictions to a more manageable number. First all three of the previously discussed criteria proposed by Inoue were filtered against and systems which

did not meet the criteria were removed. Notably this means all ternary and binary systems were removed at this stage. Predicted systems were also filtered against known BMG systems in the training data. Predicted compositions were also individually compared to BMG training compositions and removed if they were within 10% elemental composition of any BMG training point. There are 44 systems which meet these criteria, and they are summarized in *Table 4.2*.

Table 4.2. Predictions of GFA for systems constructed from elements with >250 overlap instances in training data. Systems are color coded by potential to be novel BMG (see discussion in text for color coding).

Idx	Alloy System	Size Mismatch	Minimum Mixing Enthalpy (Kj/mol)	Minimum R_C Prediction log(K/s)
1	CuFeSiZr	0.24	-85.88	1.53
2	CoCuMgZr	0.25	-27.64	1.58
3	CuMgSiZr	0.24	-80.12	1.63
4	CuFeMgZr	0.24	-14.8	1.65
5	CuNiSiZr	0.26	-90.88	1.66
6	CoCuSiZr	0.25	-89.2	1.72
7	BCuFeZr	0.81	-53.88	1.86
8	BFeMgZr	0.81	-49.68	1.88
9	BCuSiZr	0.81	-91.48	1.89
10	BCuMgZr	0.81	-46.04	1.89
11	BCuTiZr	0.81	-60.92	1.95
12	BCuNiZr	0.81	-58.52	1.98
13	CuMgTiZr	0.23	-11.32	2.00
14	BCoCuZr	0.81	-56.4	2.04
15	CuMgNiZr	0.26	-34.2	2.13
16	BCoFeZr	0.81	-61.16	2.20
17	FeMgSiZr	0.24	-82.16	2.22
18	BFeTiZr	0.81	-66.84	2.34
19	BCuNiTi	0.65	-62.24	2.36
20	CoFeSiZr	0.25	-92.36	2.40

21	CuFeTiZr	0.24	-19	2.40
22	BCuSiTi	0.65	-81.2	2.43
23	BCuMgSi	0.70	-47.64	2.56
24	CoCuTiZr	0.25	-28.48	2.57
25	BCuFeTi	0.65	-50.04	2.58
26	BFeMgSi	0.70	-56.28	2.60
27	BCuMgTi	0.70	-51.16	2.62
28	CoFeMgZr	0.25	-28.24	2.62
29	BFeMgTi	0.70	-55.76	2.67
30	BCoCuTi	0.65	-57.24	2.67
31	CoMgNiZr	0.26	-37.48	2.68
32	BFeSiTi	0.65	-80.76	2.70
33	CoMgSiZr	0.25	-85.8	2.70
34	BCoCuMg	0.70	-29.24	2.73
35	FeMgNiZr	0.26	-34.64	2.74
36	AlCoTiZr	0.25	-33.6	2.75
37	CoCuMgTi	0.17	-11.52	2.80
38	BCuFeMg	0.70	-27.8	2.81
39	FeNiSiZr	0.26	-63.04	2.82
40	BCoFeTi	0.65	-62.92	2.83
41	CoSiTiZr	0.25	-94.24	2.91
42	BCoFeMg	0.70	-34.28	2.93
43	MgNiTiZr	0.26	-30.16	2.97
44	CuFeMgSi	0.16	-38.68	3.00

As with the previous set of predictions we have grouped systems based on relative novelty. We will not discuss all systems in detail but will highlight several trends within the predicted systems as well as commenting on specific systems which may be the most novel. The 16 yellow systems are identified as containing the well-known Cu-Zr binary. Investigating their predictions further showed all predictions had increasing R_c moving away from the Cu-Zr binary suggesting that these alloys are mainly being predicted due

to adjacency to the binary. However, they still may be somewhat interesting due to changes in other materials properties while having similar R_c. Another trend in predictions is systems that suggest replacements or additions to known ternary or quaternary systems. System 19, B-Cu-Ni-Ti, is somewhat similar to the known Cu-Ni-Ti ternary and Zr-Cu-Ni-Ti quaternary BMGs systems [82,88]. One potential limitation with these systems however is with the combination of B and Ti which, as pointed out by Lin et al. may reduce GFA due to precipitation of very stable borides. They claim reduced GFA in the Zr-Cu-Ni-Ti-B quinary compared to the quaternary without Boron. System 36, Al-Co-Ti-Zr, is somewhat similar to the known Al-Co-Zr system [89], but may provide some different properties. Furthermore, there is a septenary BMG system including all of Al-Co-Ti-Zr elements, further suggesting that these elements may have good glass forming ability [90]. Because Al-Co-Ti-Zr is both a sub alloy of a BMG and has sub alloys that are BMGs it is a particularly promising system to consider. System 41, Co-Si-Ti-Zr, is one of the more distinct combinations, with no known BMGs in ternaries or quaternaries with simple replacements/additions of single elements. The most similar BMG forming alloy we could identify is reported by Ramasamy et al. in which they replace Nb with Zr In the Fe-Co-B-Si-Nb system to create Fe-Co-B-Si-Zr and report a decrease in GFA due to the replacement [91]. Finally, we identify several systems including Fe-Zr. The Fe-Zr alloy is a well-studied metallic glass though not a BMG [92]. And similar to previous systems there is a known higher component BMG system in the Fe-Co-Ni-Zr-Mo-B system[13]. Systems 19, 36, 41, and the Fe-Zr containing alloys make up all the 7 green systems in *Table 4.2*. Predicting across such a wide composition space we identified systems that build off of binary BMGs, proposed substitutions to ternary and quaternary glasses, and

also predict entirely knew alloys with no nearby known glass formers. Making predictions with such variety can hopefully inspire new synthesis and discovery of BMG alloys.

With these searches complete we take a step back to analyze in more detail our confidence in the predictions of new BMG compositions. Although our model is formally regression fit to R_c, in predicting new BMGs we have effectively used it as a classifier which predicts either BMG or not BMG if the predicted R_c is > 10^3 K/s or < 10^3 K/s, respectively. We can therefore ask the classification model question, what is the probability of an alloy actually being a BMG given that the model has predicted it to be a BMG (i.e., what is our precision)? The precision (and recall) can be estimated for our particular data by finding the true positive rate (*TPR*) and false positive rate (*FPR*) from the left-out data in the 5-fold CV tests performed in *Figure 4.3*. This yields very encouraging results, with TPR = 0.963 and FPR = 0.013. In other words, for alloys left out in a fold, the criteria R_c is < 10^3 K/s for being a BMG correctly identifies an alloy with a known R_c < 10^3 K/s 0.963 fraction of the time and finds an alloy with R_c > 10^3 K/s 0.013 fraction of the time. However, the database used here is quite different from the composition space we explore when we looked at all quaternaries made from 10 elements in the second search above. In particular, the database we are using has far more BMGs than likely in the random search, which changes the probability of correctly identifying a BMG. It is therefore necessary to correct the probability of finding a BMG derived for our database for the fact that BMGs are quite rare in our new search space. We therefore used Bayes Theorem to estimate a more accurate probability of correctly predicting a BMG from the space of relevant systems in our 10 element search. Eqn. $\Pr\left(BMG\middle|BMG_{pred}\right)$ =

$\frac{TPR*\Pr(BMG)}{TPR*\Pr(BMG)+FPR*(1-\Pr(BMG))}$. (4.2 below shows the details of Bayes theorem applied to the present calculation

$$\Pr\left(BMG\middle|BMG_{pred}\right)=\frac{TPR*\Pr(BMG)}{TPR*\Pr(BMG)+FPR*(1-\Pr(BMG))}. \quad (4.2)$$

Here $\Pr\left(BMG\middle|BMG_{pred}\right)$ is the probability of finding a BMG given that we predict a BMG, which is what we seek, and $\Pr(BMG)$ is the probability of finding a BMG from a random alloy. TPR and FPR are estimated above. $\Pr(BMG)$ is more difficult to obtain so we propose here a few methods. The first 3 methods build from DS5 and count all the BMG datapoints within the dataset. We then identify all elements which compose these BMG alloys, 41 elements total, and define a total composition space of every elemental combination up to quinary alloys in 1% composition increments. Doing this gives 838 BMG alloys in DS5 out of a total compositional space of 3.45×10^{12} potential alloys, for a probability of finding a BMG at random of 2.43×10^{-10}. This first method assumes that the 828 BMG alloys in the dataset account for all the actual BMG alloys in this entire compositional space, which is a very pessimistic assumption, and therefore serves as a lower bound on this estimate. Methods 2 and 3 modify this initial estimate as a probability ten times and one-hundred times this to represent possibilities that the current 838 known BMG alloys only comprise 10% or 1% of the actual number due to currently undiscovered alloys which could still be found in a random search. To give an upper bound on this type of analysis we also propose a fourth method taken from an estimation performed by Li et al. in which they performed a theoretical search for bulk glass formers using a number of previously established rules of thumb for identifying BMGs [36]. In

their study they estimated about 1% of syntheses of potential glassy alloys results in discovery of a BMG. This 1% estimate therefore represents the probability of randomly discovering a new BMG given that you are an expert researcher using knowledge to pick initially promising materials. Values and results for these four methods are shown in Table 4.3. Probability estimates and results for a Bayesian analysis of probabilities of finding BMGs.*Table 4.3.*

Table 4.3. Probability estimates and results for a Bayesian analysis of probabilities of finding BMGs.

Method Number	Probability of Randomly Finding BMG	ML True Positive Rate on Database	ML False Positive Rate on Database	Probability of ML Prediction being BMG
1	2.43e-10	0.963	0.013	1.77e-8
2	2.43e-9	0.963	0.013	1.77e-7
3	2.43e-8	0.963	0.013	1.77e-6
4	0.01	0.963	0.013	0.42

As noted above, the model has a TPR of 0.963 and a *FPR* of 0.013 on the database we have used for cross validation, which suggests that the trained ML model should be quite good at identifying BMG alloys from data like that used in the cross validation. However, when factoring in the overall very small population of BMG alloys within a likely search space using Eqn. 4.2 above, the probability that any predicted BMG alloy will actually be a BMG when synthesized becomes very low for methods 1, 2, and 3. These probabilities range from an approximate 10^{-8} to 10^{-6} depending on which the assumption for how many BMGs within the elemental set from DS5 have been found. This result highlights that even with fairly good cross-validated performance statistics, machine learning models are not sufficient for the discovery of new materials if the material is rare

in the search space and no human guidance is given. If now we consider method 4, in which we replace our estimate of finding a BMG with that estimated for a search space selected by domain experts, we calculate the probability that our model correctly identifies a new BMG when it predicts one to be 42%. What this result implies is that the machine learning model is likely almost useless for finding BMGs when used on random alloys, but potentially quite useful when used on a set of alloys prescreened by human experts using qualitative rules of thumb. In general, this result suggests that a hybrid approach in which machine learning models are not blindly trusted, but merged with existing domain knowledge and human selection, can massively improve the likelihood of materials discovery.

4.5. Conclusions

A machine learning model predicting critical cooling rates directly from compositional information was trained and evaluated. The training data for the model was acquired from experiments of varying leveling of fidelity with various approximations being used to combine the data in a single dataset of critical cooling rates. The model shows promising predictive ability in alloys with significant elemental representation in the training data. However, predictive ability where this overlap is low drops off considerably and the likelihood for large errors in predictions increases. Furthermore, predictions of specific composition regions within an alloy system are usually within the uncertainty of predictions which suggests that the model is likely best used for identifying potential BMG systems as opposed to searching within new systems for optimal BMG regions. Viewing the results through the lens of Bayesian statistics demonstrates that

although results seem promising the ability for these types of models to reliably predict new BMG models is significantly limited by the overall low likelihood of finding BMGs. Therefore, there is still need for improvements and tight integration with human guidance before machine learning models can be used to rapidly discover new BMGs.

Chapter 5. Other Collaborative Machine Learning Work

In addition to the main focus of this work on developing machine learning models for the prediction of critical cooling rates of metallic glasses there have also been a number of collaborative efforts which have helped to build skills and knowledge that have supported the work in Chapter 3 and Chapter 4. This chapter will briefly summarize those works, with a focus on how they have contributed to the development of the main work of this thesis.

5.1. Exploring characteristic temperatures to predict metallic glass forming ability

Note: This section has been published as L.E. Schultz, B. Afflerbach, C. Francis, P.M. Voyles, I. Szlufarska, D. Morgan, Exploration of characteristic temperature contributions to metallic glass forming ability, Comput. Mat. Sci. 196 (2021). 110494. doi:10.1016/j.commatsci.2021.110494, and has been adapted for use in this thesis.

Various combinations of characteristic temperatures, such as the glass transition temperature, liquidus temperature, and crystallization temperature, have been proposed as predictions of the glass forming ability of metal alloys. We have used statistical approaches from machine learning to systematically explore a wide range of possible characteristic temperature functions for predicting glass forming ability in the form of critical casting diameter (D_C). We explored an extensive search of features based on powers and ratios of sums and differences of characteristic temperatures (CTs), multiple machine learning models, and used nested cross validation to avoid data leakage when assessing the models. We found only weak ability for the models to predict D_C and found

that to achieve significant improvement from increasing the database size would likely require a few multiples of the present database size. Given that we are already using the largest aggregated database to date, such an increase in amount of data would likely require a very large experimental effort or application of new high-throughput approaches. We

We also found that using just Tg, Tx, and Tl directly was not statistically different than using features based on the powers and ratios of their sums and differences. These results suggest that further efforts adding terms within the examined space of features will not yield better predictive performance outside their training set compared to using the CTs directly. Some success was found in predicting D_C above or below its median value from the CTs, suggesting that they can provide some valuable D_C information. For example, models using these CTs could be used to screen small glassy samples and determine if larger glasses might be produced. Nevertheless, it appears that D_C cannot be quantified with regression models built with the set of CTs examined. Previous linear models using CTs appear to have had more success when quantifying *Rc* than D_C. This suggests that further exploration of Rc models might be more fruitful than D_C models. However, more complex models and more thorough assessment are limited by the amount of R_C data. Therefore, significant effort should be made to expand the amount of available R_C data available for future work.

5.2. Error assessment and optimal cross-validation approaches in machine learning

Note: This section has been published as H.J. Lu, N. Zou, R. Jacobs, B. Afflerbach, X.G. Lu, D. Morgan, "Error assessment and optimal cross-validation approaches in machine learning applied to impurity diffusion", Comput. Mater. Sci. 169 (2019). doi:10.1016/j.commatsci.2019.06.010, and has been adapted for use in this thesis.

In the past decade machine learning models have become widely used in materials science and engineering to identify trends in existing data and then make predictions to generate large databases, providing powerful tools for accelerating materials discovery and design. However, there is a significant need to refine approaches both for developing the best models and assessing the uncertainty in their predictions. In this work, we evaluate the performance of Gaussian kernel ridge regression (GKRR) and Gaussian process regression (GPR) for modeling ab-initio predicted impurity diffusion activation energies, using a database with 15 pure metal hosts and 408 host-impurity pairs. We demonstrate the advantages of basing the feature selection on minimizing the Leave-Group-Out (LOG) cross-validation (CV) root mean squared error (RMSE) instead of the more commonly used random K-fold CV RMSE. For the best descriptor and hyperparameter sets, the LOG RMSE from the GKRR (GPR) model is only 0.148 eV (0.155 eV) and the corresponding 5-fold RMSE is 0.116 eV (0.129 eV), demonstrating the model can effectively predict diffusion activation energies. We also show that the ab-initio impurity migration barrier can be employed as a feature to increase the accuracy of the model significantly while still yielding a significant speedup in the ability to predict the activation energy of new systems. Finally, we define r as the magnitude of the ratio of the actual error (residual) in a left-out data point during CV to the predicted standard

deviation for that same data point in the GPR model and compare the distribution of r to a normal distribution. Deviations of r from a normal distribution can be used to quantify the accuracy of the machine learning error estimates, and our results generally show that the approach yields accurate, normally distributed error estimates for this diffusion data set.

5.3. Exploring effective charge in electromigration using machine learning

Note: This section has been published as Y.-C. Liu, B. Afflerbach, R. Jacobs, S.-K. Lin, D. Morgan, "Exploring effective charge in electromigration using machine learning", MRS Commun. 9 (2019). doi:10.1557/mrc.2019.63, and has been adapted for use in this thesis.

The effective charge of an element is a parameter characterizing the electromigration effect, which can determine the reliability of interconnection in electronic technologies. In this study, a machine learning linear regression model was developed to explore the effective charge ($z*$) for electromigration of impurities in binary dilute alloy systems and pure metals at the homologous temperature of 0.9 ± 0.06. The most effective descriptors included (1) the electrical conductivity of the host element, (2) the electrical conductivity of the impurity element, (3) the periodic table column difference between the host and impurity, (4) the electronegativity difference between the host and impurity and (5) the maximum value of p valence electrons between the host and impurity, and were selected by a combination of a sequential forward selection algorithm and manual selection based on domain-specific knowledge of the physics

governing $z*$. Standard statistical analyses including the p-value, variance inflation factor, and Wald test show that these five descriptors made a significant contribution to the model, that multicollinearity of descriptors is not an issue, and that the most important descriptor is the electrical conductivity of the host, respectively. 20 iterations of 5-fold CV, leave-out alloy-group CV, and leave-out element-group CV yielded average values as follows: 5-fold CV - RMSE/σ = 0.37 ± 0.01, R2 = 0.86, leave-out alloy-group CV - RMSE/σ = 0.22 ± 0.18, R2 = 0.86, and leave-out element-group CV - RMSE/σ = 0.30 ± 0.23, R2 = 0.89, together indicating some significant predictive ability of the present model. A leave-out element-group test and a randomized test suggest the predictive ability to unknown systems, and ensures the present fitting has physical meaning, respectively. The descriptor list suggests that if the host is a good conductor and the impurity is not, with a small difference of the electronegativity between the impurity and the host, the effective charge of the impurity is expected to be a negative value. The periodic table column difference and the number of p valence electrons of the impurity makes the effective charge value more negative. The descriptors provided new information for the understanding of the origin of effective charge. Predictions of the effective charges of impurities across the periodic table within 6 often-used hosts including Al, Ag, Au, Co, Cu and Sn were made with the present model. A semi-quantitative model is obtained in the present work and the approach can be easily applied to develop improved models as new data becomes available in the future. The present machine learning model can potentially be utilized to accelerate the design of materials used in electrical interconnections and other applications where EM may play a role.

5.4. The Materials Simulation Toolkit for Machine Learning (MAST-ML): an automated open source toolkit to accelerate data drive materials research

Note: This section has been published as R. Jacobs, T. Mayeshiba, B. Afflerbach, L. Miles, M. Williams, M. Turner, R. Finkel, D. Morgan, "The Materials Simulation Toolkit for Machine learning (MAST-ML): An automated open source toolkit to accelerate data-driven materials research", Comput. Mater. Sci. 176 (2020). doi:10.1016/j.commatsci.2020.109544, and has been adapted for use in this thesis.

As data science and machine learning methods are taking on an increasingly important role in the materials research community, there is a need for the development of machine learning software tools that are easy to use (even for nonexperts with little programming background), provide flexible access to the most important algorithms, and codify best practices of machine learning model development and evaluation. Here, we introduce the Materials Simulation Toolkit for Machine Learning (MAST-ML), an open-source Python-based software package designed to broaden and accelerate the use of machine learning in materials science research. MAST-ML provides predefined routines for many input setups, model fitting, and post-analysis tasks, as well as a simple structure for executing a multi-step machine learning model workflow. Furthermore, we see MAST-ML as part of an ecosystem of open-source software contributions in the field of materials informatics. While MAST-ML currently leverages key functionality of some existing packages like matminer, MAST-ML is constantly under development, with both new features unique only to MAST-ML and broader integration with other existing and emerging software packages planned for the future. Overall, it is our desire to design tools that enable acceleration of innovative data-driven materials research. For this work

specifically development of MAST-ML has supported the custom cross validation routines, error assessment / correction, and feature generation / engineering needed to properly assess predictive ability of the machine learning models employed in Chapters 3-6.

Chapter 6. Materials Informatics Education and Undergraduate Research

Another addition to the focus of this thesis is a significant effort to develop and lead undergraduate research projects related to materials informatics as a whole. The Informatics Skunkworks is an undergraduate research group led by Professor Dane Morgan with the goal of providing authentic research experiences to undergraduates in the area materials informatics. With his support multiple opportunities have been pursued to both lead undergraduate projects as well of develop educational materials that support this effort. This work has provided opportunities to develop materials informatics knowledge and professional development skills in project management that have proved invaluable. There are three studies discussed in section 6.1, each of which highlights a development of materials informatics knowledge. These studies have not matured into published results, and therefore will be discussed at a high level with a focus on key insights that have impacted other parts of this thesis. Section 6.2 highlights the development of supporting educational materials that have been taught to over 100 undergraduate students participating in the Informatics Skunkworks Program.

6.1. Mentoring undergraduate research with the Informatics Skunkworks

6.1.1. Predicting the ductile to brittle transition temperature in irradiated steels.

Hardening of reactor pressure vessel alloys is a concern for nuclear reactor safety and lifetime extension. Commercial nuclear reactors had an initial license of 40 years, and most have now been licensed for 60 years with [93]. With Over half of the plants

beginning commercial operation between 1985 and 1996 there is additional interest in pursuing further lifetime extensions. However, there is significant difficulty in reliably predicting reactor safety and integrity past the 60-year window. In this study A gaussian process regression (GPR) was fit to predict alloy hardening as a function of alloy composition, temperature, flux, and fluence. Of particular interest is identification of domains of applicability of the trained model. Training data is obtained from three regions of irradiation flux, which is necessary for obtaining high total experimental doses of irradiation. However, predictions are of particular interest at lower flux which mirrors more closely to real world conditions in RPVs. There is also significant interest in predictions at larger total fluence, which is equivalent to longer irradiation time. Both of these tasks are in essence performing an extrapolation rather than interpolation from the training data which is something that machine learning models in general tend to struggle with. Therefore, GPR was chosen as a model in part due to its ability to automatically provide error estimation along with all predictions made by the model. These error estimations were then used to quantify when the model was uncertain of new predictions. Intermediate results from this study have helped feed into recent additions to the MAST-ML software package to support analysis of domains of applicability and assessing model error estimations.

6.1.2. Predictions of perovskite stability and bandgaps

Perovskite materials are a popular class of materials for many applications such as catalysts, solid oxide fuel cells, and photovoltaics. There has been considerable effort to use high throughput simulations of perovskite structures to calculate key parameters such as the thermodynamic phase stability and bandgap of potential materials in order to screen for potential new materials. However, the speed of these calculations using DFT is

still too slow to perform extremely wide-ranging searches for all materials of interest. One of the factors to simulation speed for bandgaps is type of functional used during the simulation. Traditional functionals such as the generalized gradient approximation (GGA) are known to often underpredict the bandgap of materials, though there are more computationally expensive functionals such as the Heyd-Scuseria-Ernzerhof hybrid functional (HSE) that can more accurately calculate them [94]. Therefore, this study pursues two approaches to obtaining machine learning predictions of perovskite bandgaps. The first is to directly predict simulated HSE bandgaps from compositional and structural information of the perovskite. The second is to use a simulated GGA bandgap value in addition to compositional and structural information as features for machine learning predictions of the HSE bandgap. This idea of using a lower fidelity dataset as input data to improve machine learning performance in predicting higher fidelity data was essential in the development of the ideas and methodology of the work in Chapter 4 in which we combine experimental data of varying levels of fidelity in order to improve machine learning predictions of metallic glass forming ability.

6.1.3. Exploring dimensionless features

A common theme in materials informatics is using compositional information as input for machine learning models. This methodology is highlighted by the work of Ward et al. who used this approach to predict a number of materials properties with elemental properties as the only source of input information [18]. This is an extremely powerful approach to model training due to the accessibility of these features. Predictions can be made instantaneously because all of the features are immediately accessible. This synergizes well with machine learning models' ability to make predictions rapidly and maintaining this accessibility is a big driving force in model development. From their

initial proposal these elemental property features have had defined multiple methods for synthesizing the individual properties from each element in a composition into one representation for the whole material. These include strategies such as taking the minimum, maximum, difference, and average of the individual elemental properties. In this study a new method is proposed to generate dimensionless combinations of the individual elemental properties. Multiple models were built to replicate results from previous machine learning work discussed in this thesis, and predictive performance was compared between a feature set using the original features generated from the MAST-ML software and the newly proposed dimensionless versions of the elemental property features. Initial results show that for random leave out cross validation tests such as K-fold cross validation both feature sets perform within error of each other. This suggests that any information included in significant relationships between the elemental features is already being successfully learned during the model fitting process. Future tests will include tests on various complexities of models, as well as different cross validation strategies.

6.2. Machine learning educational development through the Informatics Skunkworks

One of the challenges with leading undergraduate research is in training new students in the tools and techniques used in the research. As the Informatics Skunkworks grew it became more and more necessary for there to be a standard set of educational materials and curriculum for new students to complete in order to successfully participate in research activities such as those discussed in the previous section. The core of this

materials is a set of seven modules cover: python basics, overviews of common model types, introductions to model assessment with cross validation, strategies for hyperparameter optimization, and use of software packages like MAST-ML. The majority of each module is focused on an activity which mirrors common research tasks that the student may need to complete during their participation in the Informatics Skunkworks Program. Many of these concepts are covered in Chapter 1 of this thesis as they also cover the core concepts of the research presented here.

These materials have also been adapted for a number of outreach activities including being taught during the research experiences for undergraduates (REU) and research experiences for teachers (RET) summer programs enabling novice learners to pick up the basics of machine learning and get hands on experience building and training models. Modules have also been adapted and presented at two difference workshops on machine learning to give an introduction to machine learning in materials science and engineering. These workshops are highlighted in the List of Presentations.

Chapter 7. Concluding Remarks

7.1. Summary

The focus of this thesis is to address the lack of quantitative predictive models for the discovery of new metallic glasses (MGs) and bulk metallic glasses (BMGs) through prediction of the most direct measure of glass forming ability, the critical cooling rate (R_C). This lack of models has two contributing factors. First is a lack of high-quality and accessible features which can be used to train models and then make useful predictions of new alloys. Second, is a lack of experimental measurements of R_C, with existing data being limited to the order of 100 datapoints. In this work we propose and demonstrate methods to address both of these challenges.

To address the first challenge, we developed 9 computationally accessible features which can be obtained from high throughput molecular dynamics simulations of rapidly quenched alloys. These features were assessed on a computational database of R_C values which rivals the number of direct experimental R_C values. These 9 computational GFA features led to improved performance during 5-fold cross validation giving an average root mean squared error (RMSE) of 0.25 in log(R_C). Additionally, two of the newly developed features were identified as contributing the most to the improved performance; enthalpy of crystallization and icosahedral-like fraction. Both of these features can be obtained from a simulated amorphous structure improving accessibility over previously used features such as characteristic temperatures T_g, T_X, T_L which require much more time consuming experiments and or simulations to obtain accurately.

To address the second challenge of a lack of training data we develop new methods for synthesizing experimental data. By combining experimental measurements of R_C from

multiple experiment types we are able to expand the quantity of available training data by over an order of magnitude. Using this expanded dataset, we then train and assess a random forest model for the prediction of R_C from simple elemental features. Based on leave out alloy cross validation the model shows predictive errors well below an order of magnitude for alloys with significant elemental overlap in the training data. There are, however, limitations in the model's predictive ability. We note that when not predicting near known glass forming alloys predicted BMG compositions often include a wide range of compositions within an alloy system. Therefore, within each predicted new system it is often hard or impossible to identify a small region to focus any follow up experimental investigation on. Furthermore, when viewing the predictive power of the model through the lens of Bayesian statistics it is apparent that simply blindly predicting new BMG alloys is not a reasonable way to make progress as the conditional probability of any single prediction of a new BMG actually being a bulk glass is less than one in a million. With this in mind we then performed a wide search of all quaternary alloys that meet the previous overlap criteria. From this set of predictions, we identified 7 systems that not only have good ML predicted R_C values, but also met several other criteria for being potential BMG alloys. This layered approach can hopefully more successfully identify novel BMG alloys worth further study.

7.2. Suggestions for future work

Two computationally accessible features were identified in the enthalpy of crystallization and the icosahedral-like fraction of a simulated amorphous structure (See Chapter 3 for details). These features strike an important middle ground in being much more accessible than previous features such as characteristic temperatures, while still maintaining more direct information about glass forming ability than previously utilized accessible features such as elemental properties of materials [17,24]. However, there are still limitations to these types of features. The first limitation is due to the EAM potentials used during simulation. Because each interatomic potential needs to be specifically fit to a single system, rapid generation of these features for potential new metallic glasses is not possible. The most immediate avenue then to improving these features would be to successfully simulate them using ab-initio methods. The pseudo-potentials used in these methods are generated for each element and not for specific alloys, therefore it is a trivial task to explore any potential new alloy system. Currently however, the computational demands of these simulation methods may still put these features just a bit out of reach. Based on the initial study discussed in Chapter 3.5 it appears that limitations to number of atoms, and simulation time, along with complexities in approximating the correct crystal reference state prevent the enthalpy of crystallization feature from containing any useful information for predictions of GFA. However, as computational power continues to grow these types of simulated GFA features will become even more accessible, potentially improving the predictive power of future machine learning models.

Chapter 8. Appendix I

Appendix I contains supplementary information for Chapter 4.

Complete Cross Validation Analysis

For each version of the dataset 5-fold cross validation was performed to assess model performance. Because the different sub datasets are of different relative interest, we also report performance statistics in the four tables below for each sub-dataset included in DS1-DS4. Going down each row is adding more and more data to the training set, while exploring each column shows performance of both the overall performance as well as that for each dataset. Parity plots are also given in the four parity plots which show more qualitatively how the model performance is evolving as more data is included. Trends show how cross validation performance initially improves and then is maintained with additional data, with the main benefits of adding DS4 being increased selectivity in identifying potential BMGs. This is highlighted in *Figure 8.5* in which we show how predictions of the melt spun amorphous data evolves with the same dataset changes. As more data in added predictions shift dramatically. Initially more than 50% of predictions are BMGs, which would be highly unlikely. By adding the melt-spinning training points the average prediction increases and the model becomes much more selective in which materials it predicts as BMGs.

Data for predictions of each subset are included in the upper right triangle of each table and bolded to represent that they are predictions of data not included in the cross validation process at all.

Table 8.1. Complete root mean squared error (RMSE) statistics for all versions of the training data.

Dataset	Avg RMSE	DS1 RMSE	DS2 RMSE	DS3 RMSE	DS4 RMSE
DS1	1.21	1.21	**0.796**	**1.611**	**3.387**
DS1+DS2	0.669	1.221	0.461	**1.653**	**3.433**
DS1+DS2+DS3	0.719	1.082	0.478	0.928	**3.143**
DS5 = (DS1+DS2+DS3+DS4)	0.361	1.27	0.119	1.011	0.046

Table 8.2. Complete normalized root mean squared error (RMSE/σ_y) statistics for all versions of the training data.

Dataset	Avg RMSE/σ_y	DS1 RMSE/σ_y	DS2 RMSE/σ_y	DS3 RMSE/σ_y	DS4 RMSE/σ_y
DS1	0.481	0.481	**1.192**	**0.851**	**4.758**
DS1+DS2	0.539	0.486	0.691	**0.873**	**4.823**
DS1+DS2+DS3	0.501	0.43	0.715	0.49	**4.416**
DS5 = (DS1+DS2+DS3+DS4)	0.163	0.506	0.177	0.534	0.065

Table 8.3. Complete mean absolute error (MAE) statistics for all versions of the training data.

Dataset	Avg MAE	DS1 MAE	DS2 MAE	DS3 MAE	DS4 MAE
DS1	0.801	0.801	**0.634**	**1.042**	**3.026**
DS1+DS2	0.412	0.782	0.328	**1.12**	**3.061**
DS1+DS2+DS3	0.467	0.678	0.349	0.489	**2.798**
DS5 = (DS1+DS2+DS3+DS4)	0.082	0.81	0.035	0.67	0.003

Table 8.4. Complete coefficient of determination (R^2) statistics for all versions of the training data.

Training Dataset	Avg R^2	DS1 R^2	DS2 R^2	DS3 R^2	DS4 R^2
DS1	0.768	0.768	**-0.42**	**0.276**	**-21.639**
DS1+DS2	0.709	0.764	0.523	**0.238**	**-22.258**
DS1+DS2+DS3	0.749	0.815	0.489	0.76	**-18.499**
DS5 = (DS1+DS2+DS3+DS4)	0.974	0.744	0.969	0.715	0.996

Parity plots for DS1 through DS4 are shown below with datapoints color coded by data source.

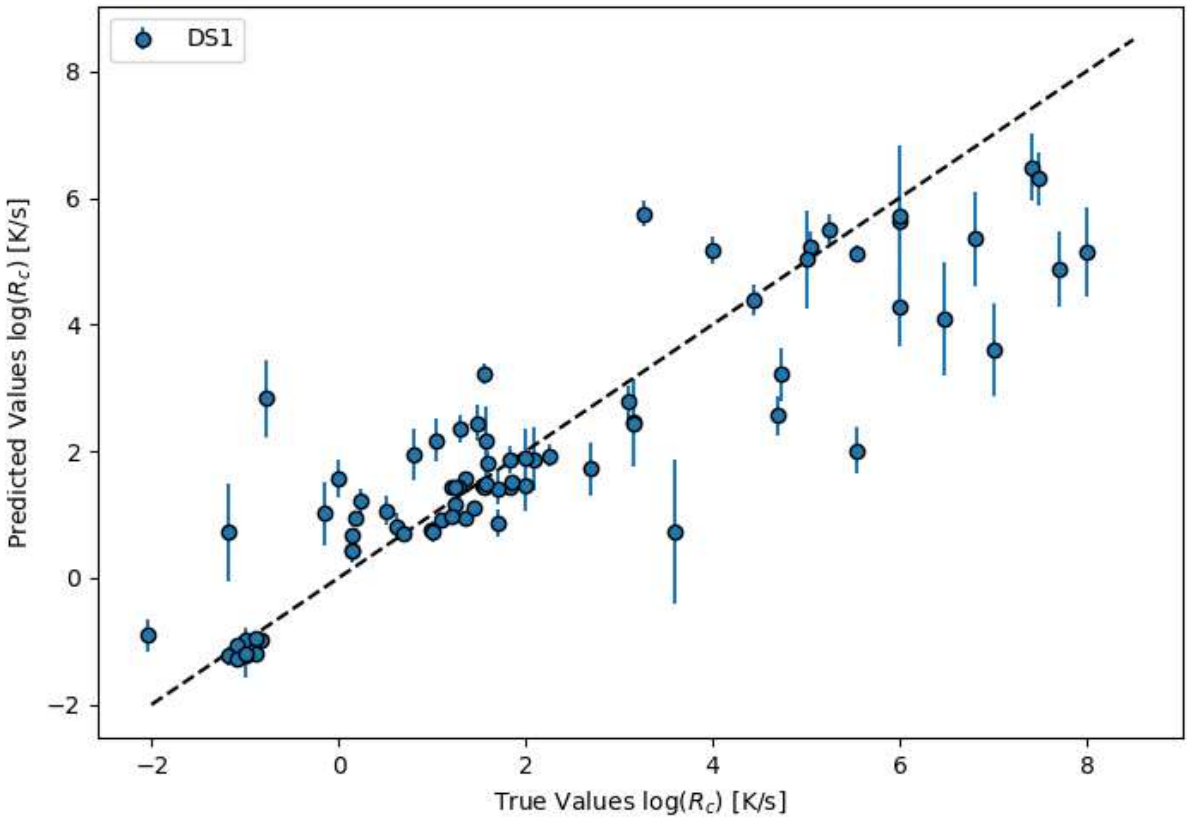

Figure 8.1. 5-Fold cross validation of the RF model color coded by data source. Model is fit only to DS1.

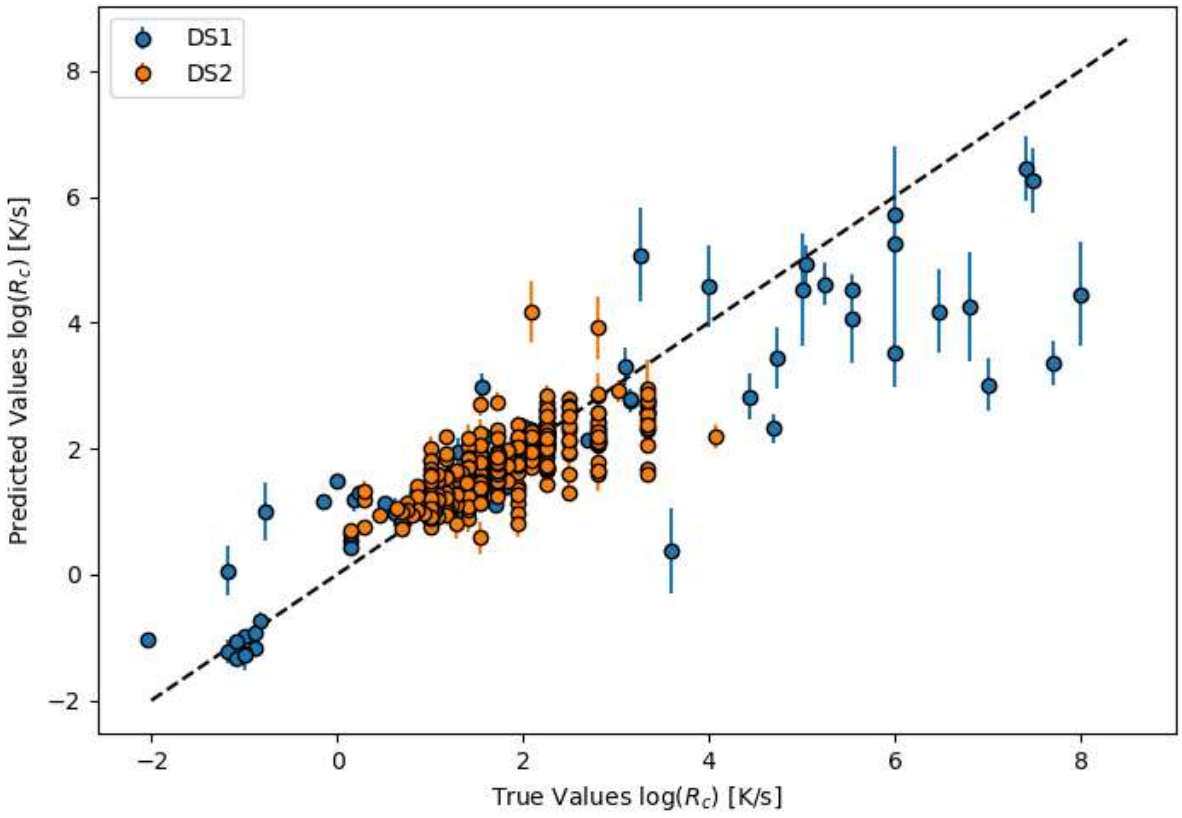

Figure 8.2. 5-fold cross validation of the RF model color coded by data source. Model is fit to DS1 and DS2.

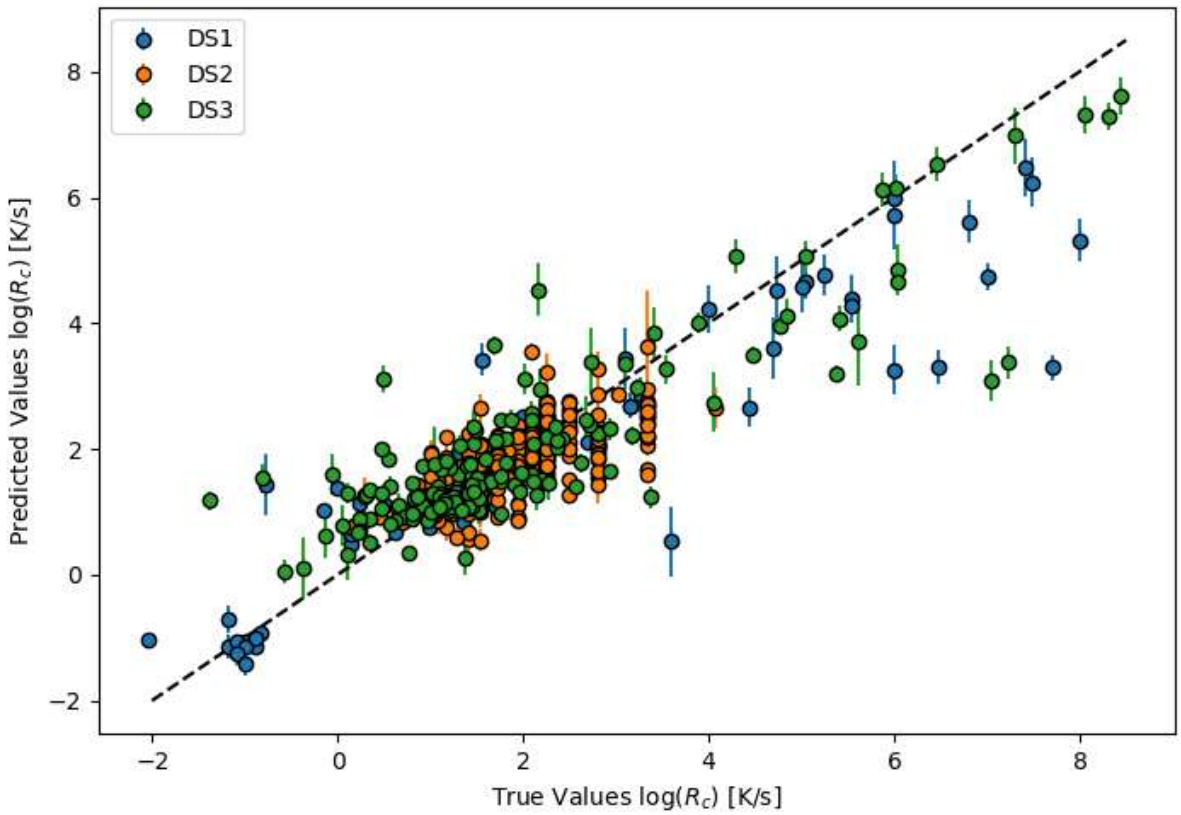

Figure 8.3. 5-fold fold cross validation of the RF model color coded by data source. Model is fit to DS1, DS2, and DS3.

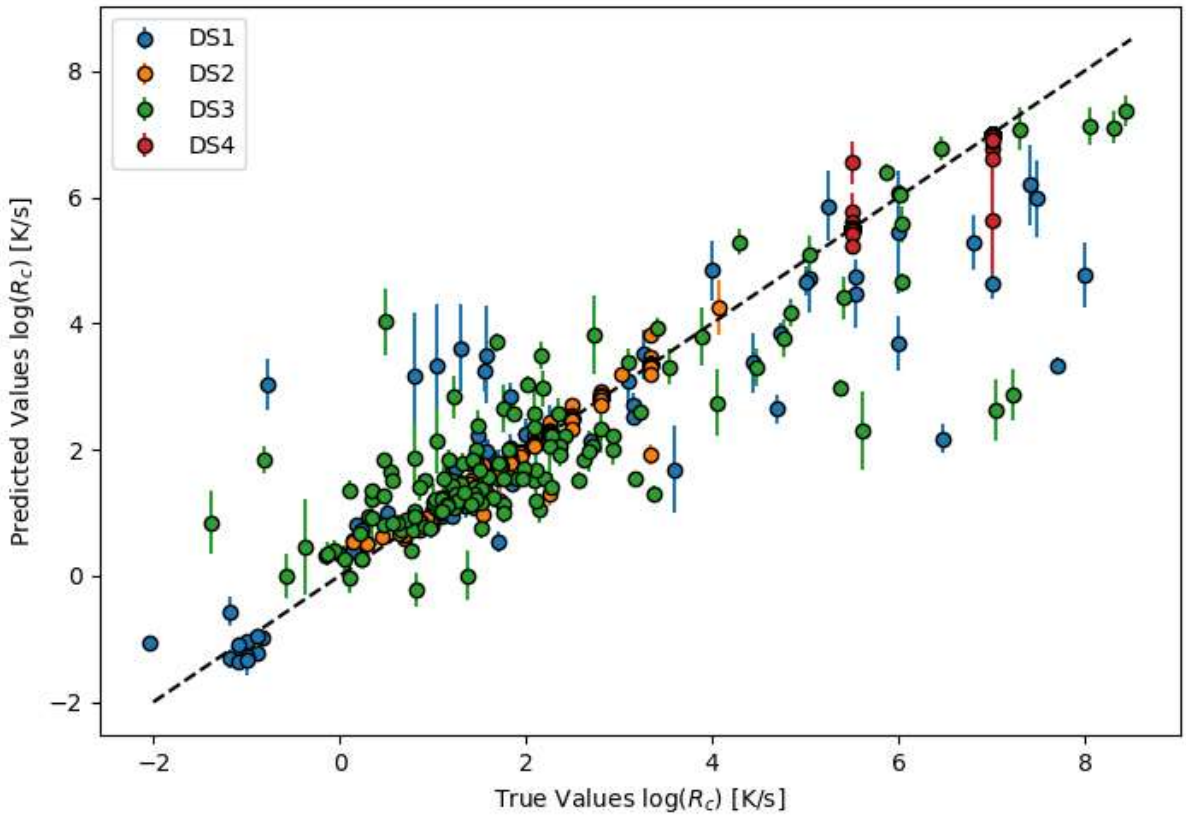

Figure 8.4. 5-Fold cross validation of the RF model color coded by data source. Model is fit to DS1, DS2, DS3, and DS4. This combination is also called DS5 for the total combined dataset

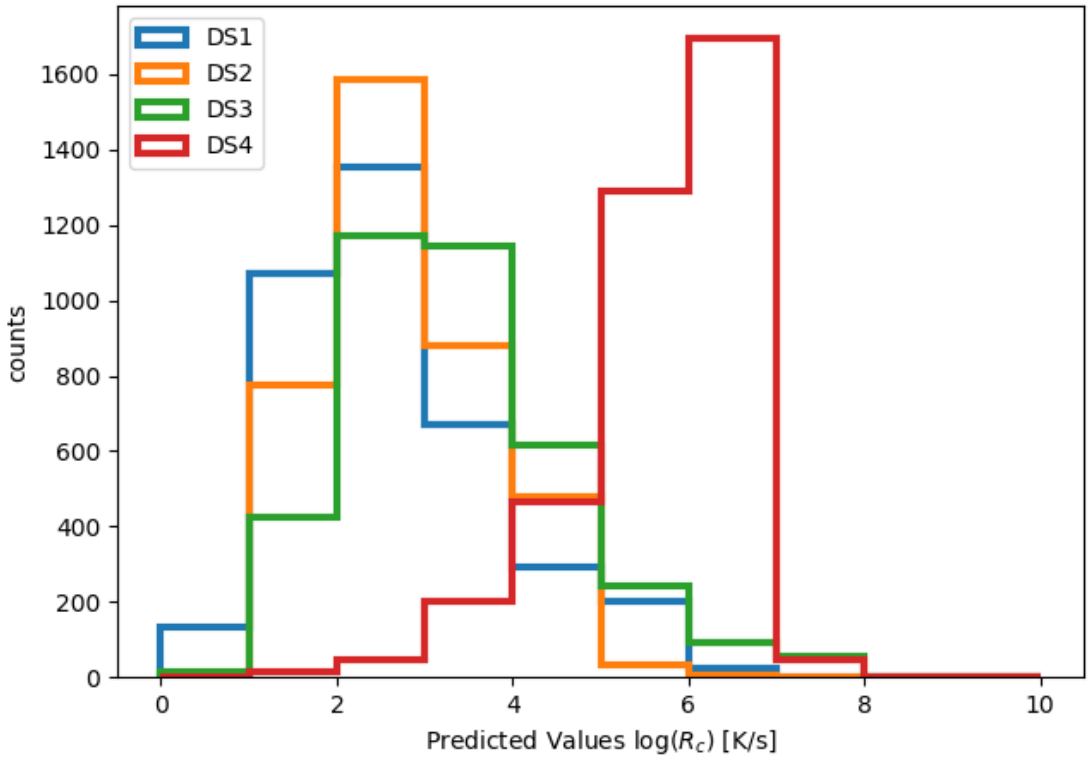

Figure 8.5. Predicted Rc values for melt-spun glasses as more data is added to the model.

Error Bar Analysis

Random Forest models generated in mast-ml also report an estimated confidence interval for each prediction which was used to generate probabilities that predictions of bulk glass formers would be accurate. To gauge the accuracy of these estimates we can generate a cumulative distribution function shown in *Figure 8.6*. This is generated during the 5-fold CV test. The x-axis is normalized to the standard deviation of the data so that a value of 1 on the x-axis represents an error of one standard deviation. The purple model errors line shows the predicted error bars on the validation data and the green residuals

line is the actual difference in predicted value and the labelled value. Comparing these two lines we can see a slight increase in predicted errors around one standard deviation on the x-axis. Overall, the errors and residuals line up very closely, demonstrating that on average they should be fairly reliable.

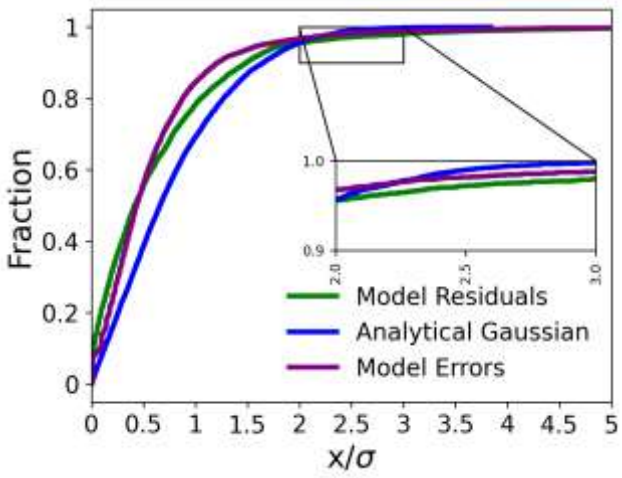

Figure 8.6. Cumulative distribution function comparing estimated model errors, residuals, and a reference gaussian distribution.

Comparison of Omega parameter with additional data points

The omega parameter used in assembly of the machine learning dataset was compared to 20 new datapoints that were produced since the original relationship was proposed. These points are divided into two categories, those with similar elemental composition to an existing point in Long's dataset, and those that are not similar. Similar datapoint were defined as those being within 5% total elemental substitution away from an existing composition. All of the new points agreed very well with the existing

relationship, demonstrating its ability to effectively convert known characteristic temperatures as expressed through omega, to an estimated critical cooling rate.

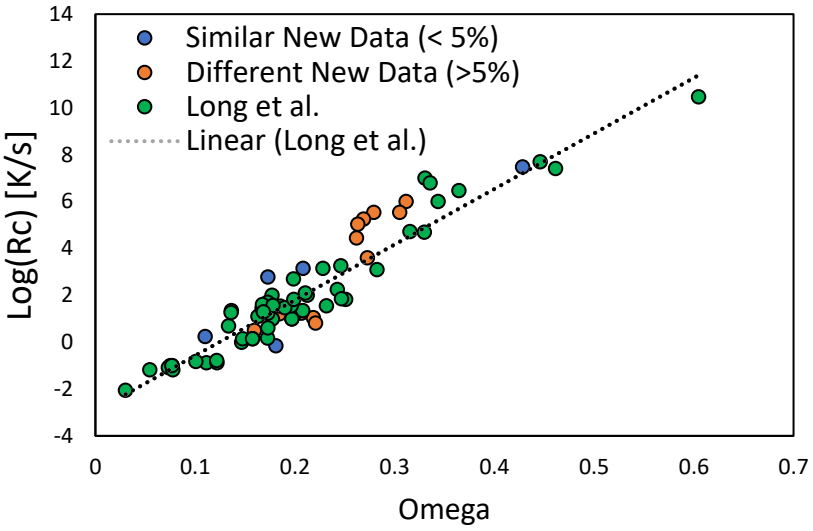

Figure 8.7. Comparison of Long's Omega relationship to new datapoints.

References

[1] P.Y. Lee, W.C. Liu, C.K. Lin, J.C. Huang, Fabrication of Mg-Y-Cu bulk metallic glass by mechanical alloying and hot consolidation, Mater. Sci. Eng. A. 449–451 (2007) 1095–1098. doi:10.1016/j.msea.2006.02.237.

[2] S.Y. Kuan, H.S. Chou, J.C. Huang, Mechanical characteristics of Mg-Cu-Zr thin film metallic glasses, Surf. Coatings Technol. 231 (2013) 58–61. doi:10.1016/j.surfcoat.2012.03.055.

[3] A. Etiemble, C. Der Loughian, M. Apreutesei, C. Langlois, S. Cardinal, J.M. Pelletier, J.F. Pierson, P. Steyer, Innovative Zr-Cu-Ag thin film metallic glass deposed by magnetron PVD sputtering for antibacterial applications, J. Alloys Compd. 707 (2017) 155–161. doi:10.1016/j.jallcom.2016.12.259.

[4] A. Inoue, Stabilization of metallic supercooled liquid and bulk amorphous alloys, Acta Mater. 48 (2000) 279–306. doi:10.1016/S1359-6454(99)00300-6.

[5] M.F. Ashby, A.L. Greer, Metallic glasses as structural materials, Scr. Mater. 54 (2006) 321–326. doi:10.1016/j.scriptamat.2005.09.051.

[6] C.A. Schuh, T.C. Hufnagel, U. Ramamurty, Mechanical behavior of amorphous alloys, Acta Mater. 55 (2007) 4067–4109. doi:10.1016/j.actamat.2007.01.052.

[7] Z. Liu, J. Schroers, General nanomoulding with bulk metallic glasses, Nanotechnology. 26 (2015) 145301. doi:10.1088/0957-4484/26/14/145301.

[8] A. Inoue, Bulk Glassy Alloys: Historical Development and Current Research, Engineering. 1 (2015) 185–191. doi:10.15302/J-ENG-2015038.

[9] A.L. Greer, K.L. Rutherford, I.M. Hutchings, Wear resistance of amorphous alloys and related materials, Int. Mater. Rev. 47 (2002) 87–112. doi:10.1179/095066001225001067.

[10] D.J. Thoma, J.H. Perepezko, A geometric analysis of solubility ranges in Laves phases, J. Alloys Compd. 224 (1995) 330–341. doi:10.1016/0925-8388(95)01557-4.

[11] J. Perepezko, R. Hebert, Amorphous aluminum alloys - Synthesis and stability, Jom-Journal Miner. Met. Mater. Soc. 54 (2002) 34–39.

[12] A. Inoue, A. Takeuchi, Recent progress in bulk glassy alloys, Mater. Trans. 43 (2002) 1892–1906. doi:10.2320/matertrans.43.1892.

[13] D.Y. Liu, W.S. Sun, H.F. Zhang, Z.Q. Hu, Preparation, thermal stability and magnetic properties of Fe-Co-Ni-Zr-Mo-B bulk metallic glass, in: Intermetallics, Elsevier, 2004: pp. 1149–1152. doi:10.1016/j.intermet.2004.04.014.

[14] W.H. Wang, Bulk metallic glasses with functional physical properties, Adv. Mater. 21 (2009) 4524–4544. doi:10.1002/adma.200901053.

[15] A. Inoue, A. Takeuchi, Bulk Metallic Glasses: Formation and Applications, Encycl. Mater. Sci. Technol. (2010) 1–6. doi:10.1016/b978-008043152-9.02236-3.

[16] B. Nair, B.G. Priyadarshini, Process, structure, property and applications of metallic glasses, Mater. 2016, Vol. 3, Pages 1022-1053. 3 (2016) 1022–1053. doi:10.3934/matersci.2016.3.1022.

[17] Z. Long, H. Wei, Y. Ding, P. Zhang, G. Xie, A. Inoue, A new criterion for predicting the glass-forming ability of bulk metallic glasses, J. Alloys Compd. 475 (2009) 207–219. doi:10.1016/j.jallcom.2008.07.087.

[18] L. Ward, A. Agrawal, A. Choudhary, C. Wolverton, A General-Purpose Machine Learning Framework for Predicting Properties of Inorganic Materials, Nat. Commun. (2015) 1–7. doi:10.1038/npjcompumats.2016.28.

[19] R. Busch, J. Schroers, W.H. Wang, Thermodynamics and kinetics of bulk metallic glass, MRS Bull. 32 (2007) 620–623. doi:10.1557/mrs2007.122.

[20] J. Wang, A. Agrawal, K. Flores, Are Hints about Glass Forming Ability Hidden in the Liquid Structure?, Acta Mater. (2019). doi:10.1016/j.actamat.2019.04.001.

[21] W.L. Johnson, J.H. Na, M.D. Demetriou, Quantifying the origin of metallic glass formation, Nat. Commun. 7 (2016) 10313. doi:10.1038/ncomms10313.

[22] B. Deng, Y. Zhang, Critical feature space for predicting the glass forming ability of metallic alloys revealed by machine learning, Chem. Phys. 538 (2020) 110898. doi:10.1016/j.chemphys.2020.110898.

[23] F. Ren, L. Ward, T. Williams, K.J. Laws, C. Wolverton, J. Hattrick-Simpers, A. Mehta, Accelerated discovery of metallic glasses through iteration of machine learning and high-throughput experiments, Sci. Adv. 4 (2018) eaaq1566. doi:10.1126/sciadv.aaq1566.

[24] L. Ward, S.C. O'Keeffe, J. Stevick, G.R. Jelbert, M. Aykol, C. Wolverton, A machine learning approach for engineering bulk metallic glass alloys, Acta Mater. 159 (2018) 102–111. doi:10.1016/j.actamat.2018.08.002.

[25] E. Fermi, J.R. Pasta, S.M. Ulam, Studies of Non-Linear Prolems (Technical Report), Collect. Work. E. Fermi. 2 (1955) 978–988.

[26] B.J. Alder, T.E. Wainwright, Studies in Molecular Dynamics. I. General Method, J. Chem. Phys. 31 (1959) 459. doi:10.1063/1.1730376.

[27] I. Štich, Correlations in the motion of atoms in liquid silicon, Phys. Rev. A. 44 (1991) 1401–1404. doi:10.1103/PhysRevA.44.1401.

[28] S.M. Foiles, M.I. Baskes, M.S. Daw, Embedded-atom-method functions for the fcc metals Cu, Ag, Au, Ni, Pd, Pt, and their alloys, Phys. Rev. B. 33 (1986) 7983–7991. doi:10.1103/PhysRevB.33.7983.

[29] T.K. Ho, Random decision forests, in: Proc. 3rd Int. Conf. Doc. Anal. Recognit., 1995: pp. 278–282 vol.1. doi:10.1109/ICDAR.1995.598994.

[30] L. Breiman, Random forests, Mach. Learn. (2001) 1–122. doi:10.1201/9780429469275-8.

[31] L. Breiman, A. Cutler, Breiman and Cutler's Random Forests for Classification and Regression, R. (2018). doi:10.1023/A.

[32] R. Tibshirani, Lasso, J. R. Stat. Soc. Ser. B. 58 (1996) 267–288.

[33] N.R. Draper, H. Smith, Applied regression analysis, John Wiley & Sons, 1998. doi:10.1002/9781118625590.

[34] M.A. Efroymson, Multiple regression analysis, Math. Method Digit. Compouters. (1960) 191–203.

[35] W. Klement, R.H. Willens, P. Duwez, Non-crystalline structure in solidified Gold-Silicon alloys, Nature. (1960). doi:10.1038/187869b0.

[36] Y. Li, S. Zhao, Y. Liu, P. Gong, J. Schroers, How Many Bulk Metallic Glasses Are There?, (2017) 687–693. doi:10.1021/acscombsci.7b00048.

[37] J. Xiong, S. Shi, T. Zhang, A machine-learning approach to predicting and understanding the properties of amorphous metallic alloys, Mater. Des. (2019) 108378. doi:10.1016/j.matdes.2019.108378.

[38] S. Plimpton, Fast Parallel Algorithms for Short – Range Molecular Dynamics, J. Comput. Phys. 117 (1995) 1–19. doi:10.1006/jcph.1995.1039.

[39] H.W. Sheng, M.J. Kramer, A. Cadien, T. Fujita, M.W. Chen, Highly optimized embedded-atom-method potentials for fourteen FCC metals, Phys. Rev. B - Condens. Matter Mater. Phys. 83 (2011) 1–20. doi:10.1103/PhysRevB.83.134118.

[40] D. Turnbull, Under what conditions can a glass be formed?, Contemp. Phys. 10 (1969) 473–488. doi:10.1080/00107516908204405.

[41] K.W. Park, J. Il Jang, M. Wakeda, Y. Shibutani, J.C. Lee, Atomic packing density and its influence on the properties of Cu-Zr amorphous alloys, Scr. Mater. 57 (2007) 805–808. doi:10.1016/j.scriptamat.2007.07.019.

[42] G.B. Bokas, L. Zhao, J.H. Perepezko, I. Szlufarska, On the role of Sm in solidification of Al-Sm metallic glasses, Scr. Mater. 124 (2016) 99–102. doi:10.1016/j.scriptamat.2016.06.045.

[43] H.W. Sheng, W.K. Luo, F.M. Alamgir, J.M. Bai, E. Ma, Atomic packing and short-to-medium-range order in metallic glasses., Nature. 439 (2006) 419–425. doi:10.1038/nature04421.

[44] S.P. Ong, W.D. Richards, A. Jain, G. Hautier, M. Kocher, S. Cholia, D. Gunter, V.L. Chevrier, K.A. Persson, G. Ceder, Python Materials Genomics (pymatgen): A robust, open-source python library for materials analysis, Comput. Mater. Sci. 68 (2013) 314–319. doi:10.1016/j.commatsci.2012.10.028.

[45] Y.Q. Jiang, P. Peng, D.D. Wen, S.C. Han, Z.Y. Hou, A DFT study on the heredity-induced coalescence of icosahedral basic clusters in the rapid solidification, Comput. Mater. Sci. 99 (2015) 156–163. doi:10.1016/j.commatsci.2014.12.024.

[46] C.E. Lekka, G.B. Bokas, G.A. Almyras, D.G. Papageorgiou, G.A. Evangelakis,

Clustering, microalloying and mechanical properties in Cu/Zr-based glassy models by molecular dynamics simulations and ab-initio computations, in: J. Alloys Compd., 2012: pp. S65--S69. doi:10.1016/j.jallcom.2011.11.038.

[47] G.B. Bokas, C.E. Lekka, D.G. Papageorgiou, G.A. Evangelakis, Microalloying effects in ternary Cu-Zr-X (X=Be, Mg, Al, Si, P, Nb, Ag) icosahedral clusters and super-clusters from Density Functional Theory computations, Polyhedron. (2017). doi:10.1016/j.poly.2017.05.001.

[48] A. Hirata, L.J. Kang, T. Fujita, B. Klumov, K. Matsue, M. Kotani, A.R. Yavari, M.W. Chen, Geometric frustration of icosahedron in metallic glasses, Science (80-.). 341 (2013) 376–379. doi:10.1126/science.1232450.

[49] D.M. Ruthven, Diffusion in zeolites, Stud. Surf. Sci. Catal. 97 (1995) 223–234. doi:10.1016/S0167-2991(06)81893-8.

[50] L. Barnard, D. Morgan, Ab initio molecular dynamics simulation of interstitial diffusion in Ni-Cr alloys and implications for radiation induced segregation, J. Nucl. Mater. 449 (2014) 225–233. doi:10.1016/j.jnucmat.2013.10.022.

[51] R. Coehoorn, G.J. Van Der Kolk, J.J. Van Den Broek, T. Minemura, A.R. Miedema, Thermodynamics of the stability of amorphous alloys of two transition metals, J. Less-Common Met. 140 (1988) 307–316. doi:10.1016/0022-5088(88)90391-8.

[52] P.K. Ray, M. Akinc, M.J. Kramer, Applications of an extended Miedema's model for ternary alloys, J. Alloys Compd. 489 (2010) 357–361. doi:10.1016/j.jallcom.2009.07.062.

[53] R. Jacobs, T. Mayeshiba, B. Afflerbach, L. Miles, M. Williams, M. Turner, R. Finkel, D. Morgan, The Materials Simulation Toolkit for Machine learning (MAST-ML): An automated open source toolkit to accelerate data-driven materials research, Comput. Mater. Sci. 176 (2020). doi:10.1016/j.commatsci.2020.109544.

[54] F. Pedregosa, G. Varoquaux, A. Gramfort, V. Michel, B. Thirion, O. Grisel, M. Blondel, P. Prettenhofer, R. Weiss, V. Dubourg, J. Vanderplas, A. Passos, D. Cournapeau, M. Brucher, M. Perrot, É. Duchesnay, Scikit-learn: Machine Learning in Python, J. Mach. Learn. Res. 12 (2012) 2825–2830. doi:10.1007/s13398-014-0173-7.2.

[55] R. Deng, Z. Long, L. Peng, D. Kuang, B. Ren, A new mathematical expression for the relation between characteristic temperature and glass-forming ability of metallic glasses, J. Non. Cryst. Solids. 533 (2020) 119829. doi:10.1016/j.jnoncrysol.2019.119829.

[56] W.Y. Liu, H.F. Zhang, A.M. Wang, H. Li, Z.Q. Hu, New criteria of glass forming ability, thermal stability and characteristic temperatures for various bulk metallic glass systems, Mater. Sci. Eng. A. 459 (2007) 196–203. doi:10.1016/j.msea.2007.01.033.

[57] W.H. Wang, C. Dong, C.H. Shek, Bulk metallic glasses, Mater. Sci. Eng. R Reports. 44 (2004) 45–90. doi:10.1016/j.mser.2004.03.001.

[58] C. Chattopadhyay, K.S.N.S. Idury, J. Bhatt, K. Mondal, B.S. Murty, Critical evaluation of glass forming ability criteria, Mater. Sci. Technol. (United Kingdom). 32 (2016) 380–400. doi:10.1179/1743284715Y.0000000104.

[59] Y.X. Zhuang, P.F. Xing, H.Y. Shi, J. Chen, P.W. Wang, J.C. He, On the heating rate dependence of crystallization temperatures of metallic glasses, J. Appl. Phys. 108 (2010). doi:10.1063/1.3457336.

[60] D. V. Louzguine-Luzgin, A.I. Bazlov, Crystallization of fcc and bcc liquid metals studied by molecular dynamics simulation, Metals (Basel). 10 (2020) 1–11. doi:10.3390/met10111532.

[61] M.-B. Tang, D.-Q. Zhao, M.-X. Pan, W.-H. Wang, Binary Cu–Zr Bulk Metallic Glasses, Chinese Phys. Lett. 21 (2004) 901.

[62] S.Y. Wu, S.H. Wei, G.Q. Guo, J.G. Wang, L. Yang, Structural mechanism of the enhanced glass-forming ability in multicomponent alloys with positive heat of mixing, Sci. Rep. 6 (2016) 38098. doi:10.1038/srep38098.

[63] W. Lu, J.C. Tseng, A. Feng, J. Shen, Structural origin of the enhancement in glass-forming ability of binary Ni-Nb metallic glasses, J. Non. Cryst. Solids. 564 (2021) 120834. doi:10.1016/j.jnoncrysol.2021.120834.

[64] H. Chen, D. Li, Y. Zhao, B. Qu, R. Zhou, B. Zhang, Structural origin of the high glass-forming ability of Ce70Ga10Cu20 alloys, Phys. Chem. Chem. Phys. 21 (2019) 4209–4214. doi:10.1039/c8cp07478j.

[65] G. Kresse, M. Marsman, ackage ienna imulation VASP the GUIDE, VASP Man. (2014).

[66] J. Xiong, T.Y. Zhang, S.Q. Shi, Machine learning prediction of elastic properties and glass-forming ability of bulk metallic glasses, MRS Commun. 9 (2019) 576–585. doi:10.1557/mrc.2019.44.

[67] Z. Li, Z. Long, S. Lei, T. Zhang, X. Liu, D. Kuang, Predicting the glass formation of metallic glasses using machine learning approaches, Comput. Mater. Sci. 197 (2021) 110656. doi:10.1016/j.commatsci.2021.110656.

[68] X. Liu, X. Li, Q. He, D. Liang, Z. Zhou, J. Ma, Y. Yang, J. Shen, Machine learning-based glass formation prediction in multicomponent alloys, Acta Mater. 201 (2020) 182–190. doi:10.1016/j.actamat.2020.09.081.

[69] J. Xiong, S.Q. Shi, T.Y. Zhang, A machine-learning approach to predicting and understanding the properties of amorphous metallic alloys, Mater. Des. 187 (2020) 108378. doi:10.1016/j.matdes.2019.108378.

[70] M.K. Tripathi, P.P. Chattopadhyay, S. Ganguly, A predictable glass forming ability expression by statistical learning and evolutionary intelligence, Intermetallics. 90 (2017) 9–15. doi:10.1016/j.intermet.2017.06.008.

[71] F. Ren, L. Ward, T. Williams, K.J. Laws, C. Wolverton, J. Hattrick-Simpers, A. Mehta, Accelerated discovery of metallic glasses through iteration of machine

learning and high-throughput experiments, Sci. Adv. 4 (2018). doi:10.1126/sciadv.aaq1566.

[72] Y.X. Zhang, G.C. Xing, Z.D. Sha, L.H. Poh, A two-step fused machine learning approach for the prediction of glass-forming ability of metallic glasses, J. Alloys Compd. 875 (2021) 160040. doi:10.1016/j.jallcom.2021.160040.

[73] P.M. Voyles, L.E. Schultz, D.D. Morgan, F. Carter, Metallic Glasses and their Properties, Mater. Data Facil. (2021). doi:https://doi.org/10.18126/nc04-ibut.

[74] Q.J. Chen, H.B. Fan, J. Shen, J.F. Sun, Z.P. Lu, Critical cooling rate and thermal stability of Fe-Co-Zr-Y-Cr-Mo-B amorphous alloy, J. Alloys Compd. 407 (2006) 125–128. doi:10.1016/j.jallcom.2005.06.031.

[75] Y. Huang, J. Shen, J.J.J. Chen, J. Sun, Critical cooling rate and thermal stability for a Ti-Zr-Ni-Cu-Be metallic glass, J. Alloys Compd. 477 (2009) 920–924. doi:10.1016/j.jallcom.2008.11.017.

[76] M. Hua, K. Won Tae, K. Do Hyang, Fabrication and mechanical properties of Mg/sub 65/Cu/sub 15 /Ag/sub 5/Pd/sub 5/Gd/sub 10/ bulk metallic glass, Mater. Trans. 44 (2003) 2141–2144.

[77] Q. Zheng, J. Xu, E. Ma, High glass-forming ability correlated with fragility of Mg–Cu(Ag)–Gd alloys, J. Appl. Phys. 102 (2007) 113519. doi:10.1063/1.2821755.

[78] J. Shen, Q. Chen, J. Sun, H. Fan, G. Wang, Exceptionally high glass-forming ability of an FeCoCrMoCBY alloy, Appl. Phys. Lett. 86 (2005) 151907. doi:10.1063/1.1897426.

[79] H. Davies, Rapid quenching techniques and formation of metallic glasses, Rapidly Quenched Met. III. 1 (1978) 1–21.

[80] S. Mukherjee, H.-G. Kang, W.L. Johnson, W.-K. Rhim, Noncontact measurement of crystallization behavior, specific volume, and viscosity of bulk glass-forming Zr-Al-Co-(Cu) alloys, Phys. Rev. B. 70 (2004) 174205. doi:10.1103/PhysRevB.70.174205.

[81] N. Liu, T. Ma, C. Liao, G. Liu, R. Miguel, O. Mota, J. Liu, S. Sohn, S. Kube, S. Zhao, J.P. Singer, Combinatorial measurement of critical cooling rates in aluminum - base metallic glass forming alloys, Sci. Rep. (2021) 1–9. doi:10.1038/s41598-021-83384-w.

[82] X.H. Lin, W.L. Johnson, Formation of Ti-Zr-Cu-Ni bulk metallic glasses, J. Appl. Phys. 78 (1995) 6514–6519. doi:10.1063/1.360537.

[83] D.B. Miracle, D. V. Louzguine-Luzgin, L. V. Louzguina-Luzgina, A. Inoue, An assessment of binary metallic glasses: Correlations between structure, glass forming ability and stability, Int. Mater. Rev. 55 (2010) 218–256. doi:10.1179/095066010X12646898728200.

[84] P. Horvath, modAL: A modular active learning framework for Python, (n.d.) 1–5.

[85] J. Schroers, B. Lohwongwatana, W.L. Johnson, A. Peker, Gold based bulk metallic

glass, Appl. Phys. Lett. 87 (2005) 404–406. doi:10.1063/1.2008374.

[86] A. Takeuchi, A. Inoue, Calculations of mixing enthalpy and mismatch entropy for ternary amorphous alloys, Mater. Trans. JIM. 41 (2000) 1372–1378. doi:10.2320/matertrans1989.41.1372.

[87] P. Villars, H. Okamoto, K. Cenzual, ASM Alloy Phase Diagrams Database, (2016). http://www.asminternational.org.ezproxy.library.wisc.edu.

[88] P. Gargarella, S. Pauly, K.K. Song, J. Hu, N.S. Barekar, M. Samadi Khoshkhoo, A. Teresiak, H. Wendrock, U. Kühn, C. Ruffing, E. Kerscher, J. Eckert, Ti-Cu-Ni shape memory bulk metallic glass composites, Acta Mater. 61 (2013) 151–162. doi:10.1016/j.actamat.2012.09.042.

[89] X.F. Zhang, Y.M. Wang, J.B. Qiang, Q. Wang, D.H. Wang, D.J. Li, C.H. Shek, C. Dong, Optimum Zr-Al-Co bulk metallic glass composition Zr53Al 23.5Co23.5, in: Intermetallics, Elsevier, 2004: pp. 1275–1278. doi:10.1016/j.intermet.2004.07.004.

[90] T. Wada, J. Jiang, K. Yubuta, H. Kato, A. Takeuchi, Septenary Zr–Hf–Ti–Al–Co–Ni–Cu high-entropy bulk metallic glasses with centimeter-scale glass-forming ability, Materialia. 7 (2019) 100372. doi:10.1016/j.mtla.2019.100372.

[91] P. Ramasamy, M. Stoica, S. Bera, M. Calin, J. Eckert, Effect of replacing Nb with (Mo and Zr) on glass forming ability, magnetic and mechanical properties of FeCoBSiNb bulk metallic glass, J. Alloys Compd. 707 (2017) 78–81. doi:10.1016/j.jallcom.2016.11.408.

[92] Z. Altounian, C.A. Volkert, J.O. Strom-Olsen, Crystallization characteristics of Fe-Zr metallic glasses from Fe 43Zr57 to Fe20Zr80, J. Appl. Phys. 57 (1985) 1777–1782. doi:10.1063/1.334455.

[93] How old are U.S. nuclear power plants, and when was the newest one built?, U.S. Energy Inf. Adm. (2021). https://www.eia.gov/tools/faqs/faq.cfm?id=228&t=21.

[94] J. Heyd, G.E. Scuseria, M. Ernzerhof, Hybrid functionals based on a screened Coulomb potential, J. Chem. Phys. 118 (2003) 8207–8215. doi:10.1063/1.1564060.